RESEARCH ARTICLE

Particulate matter exposure and chronic cerebral hypoperfusion promote oxidative stress and induce neuronal and oligodendrocyte apoptosis in male mice

Krista Lamorie-Foote[1,2] | Qinghai Liu[1] | Kristina Shkirkova[1] | Brandon Ge[1] |
Shannon He[1] | Todd E. Morgan[3] | Wendy J. Mack[4] | Constantinos Sioutas[5] |
Caleb E. Finch[3] | William J. Mack[1,2]

[1]Zilkha Neurogenetic Institute, University of Southern California, Los Angeles, California, USA

[2]Department of Neurological Surgery, Keck School of Medicine, University of Southern California, Los Angeles, California, USA

[3]Leonard Davis School of Gerontology, University of Southern California, Los Angeles, California, USA

[4]Department of Population and Public Health Sciences, University of Southern California, Keck School of Medicine, Los Angeles, California, USA

[5]Department of Civil and Environmental Engineering, Viterbi School of Engineering, University of Southern California, Los Angeles, California, USA

Correspondence
Krista Lamorie-Foote, Zilkha Neurogenetic Institute, University of Southern California, 1975 Zonal Avenue, Los Angeles, CA 90033, USA.
Email: lamorief@usc.edu

Funding information
National Institute of Environmental Health Sciences, Grant/Award Number: #R01ES024936; National Institute on Aging, Grant/Award Number: #P01AG055367; National Institutes of Health, Grant/Award Number: RF1NS130681

Abstract

Chronic cerebral hypoperfusion (CCH) may amplify the neurotoxicity of nanoscale particulate matter (nPM), resulting in white matter injury. This study characterized the joint effects of nPM (diameter ≤ 200 nm) and CCH secondary to bilateral carotid artery stenosis (BCAS) exposure on neuronal and white matter injury in a murine model. nPM was collected near a highway and re-aerosolized for exposure. Ten-week-old C57BL/6 male mice were randomized into four groups: filtered air (FA), nPM, FA + BCAS, and nPM + BCAS. Mice were exposed to FA or nPM for 10 weeks. BCAS surgeries were performed. Markers of inflammation, oxidative stress, and apoptosis were examined. nPM + BCAS exposure increased brain hemisphere TNFα protein compared to FA. iNOS and HNE immunofluorescence were increased in the corpus callosum and cerebral cortex of nPM + BCAS mice compared to FA. While nPM exposure alone did not decrease cortical neuronal cell count, nPM decreased corpus callosum oligodendrocyte cell count. nPM exposure decreased mature oligodendrocyte cell count and increased oligodendrocyte precursor cell count in the corpus callosum. nPM + BCAS mice exhibited a 200% increase in cortical neuronal TUNEL staining and a 700% increase in corpus callosum oligodendrocyte TUNEL staining compared to FA. There was a supra-additive interaction between nPM and BCAS on cortical neuronal TUNEL staining (2.6× the additive effects of nPM + BCAS). nPM + BCAS exposure increased apoptosis, neuroinflammation, and oxidative stress in the cerebral cortex and corpus callosum. nPM + BCAS exposure increased neuronal apoptosis above the separate responses to each exposure. However, oligodendrocytes in the corpus callosum demonstrated a greater susceptibility to the combined neurotoxic effects of nPM + BCAS exposure.

- -

1 | INTRODUCTION

Particulate matter (PM) exposure is associated with an increased risk of dementia and cognitive decline in experimental and epidemiological studies (Cacciottolo et al., 2017; Chen et al., 2017; Kulick et al., 2020; Peters et al., 2019; Petkus et al., 2020; Tsai et al., 2019; Younan et al., 2020). Patients with underlying neurologic disease may be more susceptible to the toxic effects of PM (Block et al., 2012). One study has demonstrated that exposure to re-aerosolized nPM (PM ≤ 200 nm) collected from Los Angeles increased infarct volumes by 1.8-fold following murine stroke (Liu et al., 2016). Cerebral hypoperfusion can lead to neurodegeneration and white matter injury (Crane et al., 2015; Dominguez et al., 2018; Kim, Alvarado, et al., 2020; Liu et al., 2013; Patel et al., 2017; Sweeney et al., 2019; van Dalen et al., 2016). In patients with mild cognitive impairment, reduced cerebral blood flow is associated with increased white matter lesion volume (Kim, Alvarado, et al., 2020). We have shown that the combination of nPM exposure and chronic cerebral hypoperfusion (CCH) secondary to bilateral carotid artery stenosis (BCAS) caused synergistic white matter injury in a murine model (2.3 times the additive effects of nPM and CCH exposure) (Liu et al., 2021). nPM and CCH exposures may induce this neurotoxicity through shared inflammatory pathways and oxidative stress.

Joint nPM and BCAS exposure induces a potent inflammatory response, with microglial activation and upregulation of the TLR4 signaling pathway and complement cascade (Liu et al., 2021). This inflammatory response may increase tumor necrosis factor alpha (TNFα) and inducible nitric oxide synthase (iNOS) production. Upregulation of iNOS generates nitric oxide (NO), which can be neurotoxic at high levels (Garry et al., 2015). Chronic increases in NO and other oxidative stressors can overwhelm the antioxidant capacity of cells and cause oxidative damage (Liguori et al., 2018). Oxidative stress byproducts, including 4-hydroxynonenal (4-HNE), can activate apoptosis via intrinsic or extrinsic pathways (Bertheloot et al., 2021; Dalleau et al., 2013; Zhang et al., 2017). Excessive apoptosis has been implicated in Alzheimer's disease, Parkinson's disease, and amyotrophic lateral sclerosis (Kano et al., 2018; Radi et al., 2014).

White matter may be preferentially susceptible to the neurotoxic effects of PM and CCH exposures (Babadjouni et al., 2018; Calderón-Garcidueñas et al., 2008; Chen et al., 2015, 2020; Kim, Kim, et al., 2020; Woodward, Pakbin, et al., 2017). Previous studies showed associations between increased residential $PM_{2.5}$ exposure and white matter loss (Chen et al., 2015, 2020; Erickson et al., 2020). The properties of myelin, oligodendrocytes, and in particular oligodendrocyte precursor cells (OPCs), render white matter uniquely vulnerable to oxidative damage (Giacci et al., 2018; Lassmann & van Horssen, 2016; Thorburne & Juurlink, 1996). Myelin sheaths

Significance

Air pollution particulate matter exposure (PM) has been associated with an increased risk of dementia. Patients with underlying neurological disease may be uniquely vulnerable to PM neurotoxicity. The present study demonstrates that combined PM exposure and chronic cerebral hypoperfusion causes neuronal and oligodendrocyte cell death, with the greatest injury in oligodendrocytes. Our results suggest a supra-additive interaction between an environmental exposure and underlying cerebrovascular disease.

have a high lipid content, while oligodendrocytes have a high metabolic rate, increased iron content, and low levels of antioxidants (Giacci et al., 2018; Lassmann & van Horssen, 2016; Thorburne & Juurlink, 1996). Furthermore, oxidative stress can disrupt OPC differentiation and impair remyelination (Lloret et al., 2021; Miyamoto et al., 2013; Spaas et al., 2021). We previously demonstrated myelin damage, gross white matter injury, and decreased corpus callosum volumes in mice exposed to nPM and BCAS (Liu et al., 2021).

Zhang et al. reported decreases in potency of recent Los Angeles nPM batches since 2018 (Zhang et al., 2021). This study evaluates the neurotoxicity of nPM batches collected before the observed decrease in batch activity. The present study leverages a murine model of nPM and BCAS to characterize the differential effects of joint nPM and CCH exposure on neuronal and white matter toxicity. Apoptosis and cell death are assessed in oligodendrocytes in the corpus callosum and neurons in the cerebral cortex. Markers related to inflammation and oxidative stress are examined.

2 | MATERIALS AND METHODS

2.1 | Study design

All procedures were approved by the University of Southern California Institutional Animal Care and Use Committee (IACUC) and performed in accordance with the Guide for the Care and Use of Laboratory Animals (NIH). Male C57BL/6J mice aged 10 weeks purchased from Jackson Laboratory were group housed in a barrier facility with access to food and water on a 12-h light dark cycle, except during the nPM/filtered air exposures. Mice were randomized to four exposure groups: filtered air (FA), nPM, FA + BCAS, or nPM + BCAS (n = 40). Of the 40 total mice, a cohort (n = 16) was designated a

priori to undergo western blot analysis, while an additional cohort ($n = 24$) was designated to undergo immunofluorescence and TUNEL analyses. Investigators were masked to the exposure allocation. Mice were exposed to FA or re-aerosolized nPM for 5 h/day, 3 days/week for 10 weeks (150 h). BCAS surgeries were performed 30 days prior to the end of the exposure. Mice that died during the exposure period were excluded from analysis.

Mice were humanely euthanized within 72 h of the last exposure. A thoracotomy and cardiotomy were performed while mice were deeply anesthetized with an intraperitoneal injection of ketamine (80–200 mg/kg) and xylazine (5–20 mg/kg). Mice were transcardially perfused with PBS and heparin (5 U/ml). For immunofluorescence and terminal deoxynucleotidyl transferase dUTP nick end labeling (TUNEL) analyses, a fixative solution (10% paraformaldehyde in .01 mol/L PBS buffer) was then perfused. Brains were stored in 4% paraformaldehyde for 24 h at 4°C, dehydrated in ethanol (70%), and paraffin embedded. For western blot analysis, brains were flash frozen with liquid nitrogen and stored at −80°C.

2.2 | Particulate matter collection

Nanoscale particulate matter (nPM; particles with aerodynamic diameter < 200 nm) was collected from a Los Angeles area impacted by traffic emissions following a previously described protocol (Misra et al., 2002; Woodward, Levine, et al., 2017). A high-volume ultrafine particle sampler collected nPM at 400 L/min using a multiple rectangular (slit) geometry jet conventional impactor that removed particles greater than 200 nm (Misra et al., 2002). nPM was collected on pretreated Teflon filters (8 × 10″, PTFE, 2 m pore) and transferred into an aqueous suspension by the soaking of filters for 30 min in Milli-Q deionized water (resistivity, 18.2 MW; total organic compounds <10 ppb; particle free; endotoxin levels <1 units/ml; endotoxin-free glass vials). nPM was resuspended by vortexing (5 min) and sonication (30 min). In accordance with US Environmental Protection Agency recommended procedures, aqueous suspensions were pooled and frozen at −20°C (Biran et al., 1996). Endotoxin was not detected in these nPM suspensions by the *Limulus* amebocyte assay (LPS < .02EU/ml). As a control, sterile filters were extracted in a similar manner and stored.

The current experiments were performed on mice exposed to nPM batches collected in 2015, 2016 (batches 2015a, 2016a), and 2017 (batch ID 5). According to Zhang et al., each of these batches demonstrated standard nPM potency (Zhang et al., 2021).

2.3 | Particulate matter exposure

For exposures, nPM was re-aerosolized using a HOPE nebulizer (Model 11310, B&B Medical Technologies, Carlsbad, CA, USA) with compressed HEPA-filtered air. Throughout the exposure, particle size and concentration were monitored with a scanning mobility particle sizer (SMPS model 3080; TSI Inc., Shoreview, MN). The

average nPM mass concentration was maintained at approximately 330 ($\pm$25) μg/m^3, roughly twice that of heavily trafficked highways (Morgan et al., 2011). Out of the total 15 1/min of aerosol flow generated, 10 1/min was drawn through the exposure chamber, while 5 1/min was redirected to filters and obtained for particle characterization. A Teflon filter was weighed pre- and postexposure under controlled temperature and relative humidity to determine nPM mass concentration. Inorganic ions (ammonium (NH_4^+), nitrate (NO_3^-), sulfate (SO_4^{2-})), and PM-bound metals/trace elements were analyzed with ion chromatography and magnetic-sector inductively coupled plasma mass spectroscopy, respectively. Water-soluble organic carbon was collected on a quartz filter and analyzed using a GE-Sievers liquid analyzer (GE-Sievers, Boulder, CO). Mice were placed in temperature and air controlled whole-body exposure chambers to ensure adequate ventilation during the exposure.

2.4 | nPM characteristics

nPM composition was analyzed to determine the exposure aerosol size and chemical composition associated with the present study's results. During the 150 h of exposure, the average mass concentration was 312 ± 18 μg/m^3, and the average particle number concentration (PNC) was 3.6 ($\pm$.11) * 10^5 particles/cm^3. Total organic carbon was the most predominant chemical species, accounting for 49 ($\pm$8) % of total mass. The mass fractions of each of the trace elements and metals are listed in Table 1. The size distribution of the exposure aerosol is presented in Table 2. According to the table, the mode diameter is around 50 ($\pm$10) nm which is typical of particulate matter in the urban areas impacted by traffic emissions (Pirhadi et al., 2020; Sowlat et al., 2016). nPM composition and size distribution were similar across nPM batches used in this study (Tables 1 and 2). The characteristics of the exposure aerosol were representative of a sample collected from an urban area impacted by traffic emissions, with total organic matter being the most predominate constituent of PM (Hasheminassab, Daher, Ostro, & Sioutas, 2014).

2.5 | Bilateral carotid artery stenosis

BCAS surgeries were performed 30 days prior to the end of the exposure period as previously described (Liu et al., 2013, 2021; Shibata et al., 2004). Mice were anesthetized with an intraperitoneal injection of Ketamine (80–100 mg/kg) and Xylazine (5–10 mg/kg). Rectal temperature was maintained at 36.5–37°C throughout the procedure. Mice were placed in the prone position. A Laser Doppler Flowmetry microtip fiber probe was fixed to the skull (Probe 418-1 master probe PF 5010 Laser Doppler Perfusion Monitoring Unit, Perimed AB, Sweden) 1 mm posterior and 5 mm left of the bregma to monitor cerebral blood flow (CBF). Mice were then placed in a supine position. The bilateral common carotid arteries were exposed through a midline cervical incision. An external microcoil was applied to each common carotid artery (.18 mm diameter, 2.5-mm length)

TABLE 1 Mass fractions of organic carbon, trace elements, and metals (ng/μg of PM mass) during exposures

Species	Exposure 1	Exposure 2	Exposure 5
Total organic carbon (TOC)	395.7	312.9	202.6
S	37.70	37.40	8.70
Na	36.88	36.25	6.71
Ca	33.28	30.26	11.28
Mg	10.34	8.29	1.98
Al	8.85	.34	4.70
Fe	8.65	.08	3.56
K	6.67	5.51	1.79
Zn	2.98	2.60	1.51
P	.99	.40	1.16
Ba	.75	.46	.00
Cu	.58	.29	.34
Ti	.35	.01	.23
Mn	.33	.24	.06
B	.30	.28	.09
Ni	.26	.20	.07
Cr	.165	.019	.059
Sb	.126	.099	.210
Pb	.110	.005	1.023
Sn	.066	.008	.002
Mo	.054	.044	.078
Se	.045	.039	.006
V	.038	.020	.011
Li	.016	.011	.005
Rb	.014	.006	.005
As	.014	.010	.003
Co	.012	.008	.003
Ce	.007	.000	.002
La	.004	.000	.215
Cd	.004	.003	.001

(Sawane company, Japan). CBF values were recorded prior to surgery and after each microcoil application. The incisions were closed and mice recovered in a temperature-controlled environment with ready access to food and water. Subcutaneous carprofen (5 mg/kg) was administered 24 and 48 h postoperatively.

2.6 | Western blot

Brains were harvested, weighed, and one hemisphere of each brain (not including the midbrain, pons, or medulla) was isolated for TNFα western blot analysis. Brains were suspended in 1 ml Neuronal Protein Extraction Reagent (Thermo Scientific, 87792) buffer with added protease inhibitors (Roche complete mini protease inhibitor cocktail tablets, Sigma, 4693124001, 1:10). Tissue was homogenized and incubated for 10 min on ice. Samples were centrifuged at 10,000g for 10 min and lysates were removed. The Pierce BCA Protein Assay Kit was used to measure the supernatant protein concentration. Tissue samples were separated by SDS-PAGE and transferred to a nitrocellulose membrane. The membrane was blocked in 5% nonfat milk for 1 h, incubated overnight in primary TNFα (1:1000, Cell Signaling 11948, RRID:AB_2687962) antibody, and washed with TBS-Tween*-20 (Table S1). Subsequently, the membrane was incubated in secondary antibody (1:4000, anti-rabbit IgG, Bio-Rad 170-6515, RRID:AB_11125142) in 5% nonfat milk in TBS-Tween-20. GE Healthcare ECL prime western blotting detection reagent was used and blots were imaged with a CCD camera. TNFα and GAPDH (1:20,000, Sigma, RRID:AB_796208) protein levels and relative densities were measured using NIH Image J software (Table S1). Background was subtracted and TNFα relative density was normalized to GAPDH.

2.7 | Immunofluorescence

Paraffin-embedded brains were sliced into 5-μm-thick coronal sections from 1 mm anterior to the bregma to 2 mm posterior to the bregma. Sections were deparaffined and rehydrated using a

TABLE 2 Exposure number and the corresponding data analysis

Exposure number	nPM collection dates	PM mass concentration[a] (μg/m³)	Total PNC[b] (#/cm³)	PN mode diameter (nm)	TOM%[c] (μg TOM/ μg PM mass)	Mortality rate (%)
1 (batch 2015a)[d]	October–December 2015	330	357,969	53.3	63.3 ± 7.8	0 (0/36)
2 (batch 2016a)[d]	February–April 2016	295	348,341	57.3	50.1 ± 6.2	30.6 (11/36)
5 (batch 5)[d]	May–June 2017	310	370,414	50.6	32.4 ± 4.4	19.4 (7/36)

Abbreviations: PM, particulate matter; PNC, particle number concentration; TOC, total organic carbon; TOM, total organic matter.

[a]The average values reported for PM are the average of our DustTrack observations in the mid-way of each exposure day.

[b]Total PNC values are recorded by SMPS for each nPM batch used for the inhalation exposure in the beginning of each exposure campaign.

[c]To account for the contributions of non-carbon atoms (e.g., oxygen, hydrogen) and effect of PM oxygenation in the ambient through photochemistry, total mass of organic matter (OM) is reported by multiplying TOC% by a factor of 1.6 recommended for urban aerosols (Turpin & Lim, 2001).

[d]nPM batch numbers reference those listed in Zhang et al (Zhang et al., 2021).

series of ethanol dilutions (100%–70%). Antigen was retrieved with Dako antigen retrieval solution (iNOS), or 10 mM sodium citrate (Olig2, NeuN, 4-HNE, cyclic nucleotide phosphodiesterase (CNPase), platelet-derived growth factor α (PDGFRα)). Sections were blocked with 5% donkey serum for 1 h and incubated overnight with primary antibodies. The following primary antibodies were used: anti-NeuN (anti-mouse, 1:200, Millipore Sigma MAB377, RRID:AB_2814948), a marker for neurons; anti-Olig2 (anti-goat, 1:200, R&D Biosystems AF2418, RRID:AB_2157554), a marker for oligodendrocytes; anti-CNPase (anti-rabbit, 1:1000, Cell Signaling 5564, RRID:AB_10705455), a marker for myelinated mature oligodendrocytes (mOL); anti-PDGFRα (anti-rabbit, 1:50, Cell Signaling 3174, RRID:AB_2162345), a marker for oligodendrocyte precursor cells (OPCs); anti-iNOS (anti-rabbit, 1:200, Novus Biologicals NB300-605) and anti-4-HNE (anti-mouse, 1:150, R&D Biosystems MAB3249, RRID:AB_664165), markers for oxidative stress (Table S1). Subsequently, sections were incubated with secondary antibodies Alexa Fluor 568 (1:200, Thermo Fisher A10037, RRID:AB_2534013 or 1:200, Thermo Fisher A10042, RRID:AB_2534017) or Alexa Fluor 488 (1:200, Thermo Fisher A11055, RRID:AB_2534102 or 1:200, Thermo Fisher, RRID:AB_141607) for 1 h. For Olig2 and NeuN, the TUNEL assay was then performed. For iNOS, 4-HNE, Olig2 + CNPase double immunostaining, and Olig2 + PDGFRα double immunostaining, nuclei were stained with Hoechst 33342 for 10 min. Dako fluorescent mounting media were used to mount slides. Sections were coverslipped and imaged with BZ-9000 florescent microscopy (Keyence, NJ). Mean integrated densities of iNOS and 4-HNE were quantified in the medial corpus callosum and the frontal cerebral cortex (in the same region as TUNEL analyses). Reviewers quantified Olig2 + CNPase and Olig2 + PDGFRα double-positive cell counts in the medial corpus callosum using NIH Image J software. Two masked reviewers performed all analyses and their results were averaged. Immunofluorescence values from the right and left corpus callosum and the right and left cortex were averaged.

2.8 | Terminal deoxynucleotidyl transferase dUTP nick end labeling (TUNEL)

Apoptosis was measured using the terminal deoxynucleotidyl transferase dUTP nick end labeling (TUNEL) assay. The TUNEL assay stains 3-hydroxyl termini of double-stranded DNA breaks, which can be formed during apoptosis (Mirzayans & Murray, 2020). Following Olig2 and NeuN immunostaining, the TUNEL assay was performed per the manufacturer's instructions (Roche, catalog #11684795910). Briefly, the positive control was incubated with DNase I recombinant (3000 U/mL-3 U/mL in 50 mM Tris–HCl, pH 7.5, 1 mg/mL BSA) for 10 min to induce DNA strand breaks. Slides were incubated with TUNEL reaction mixture for 60 min in a humidified atmosphere at 37°C. The negative control was incubated in a solution without terminal transferase. Slides were washed and incubated with Hoechst 33342 for 10 min to stain nuclei. Sections were mounted with Dako fluorescent mounting media, coverslipped, and imaged in the corpus callosum and the watershed region of the cortex using BZ-9000 florescent microscopy (Keyence, NJ).

All sections for assessed outcomes were analyzed at 400× magnification. The regions of interest for all analyses included the medial corpus callosum (right and left side) and the frontal cerebral cortex (right and left, layers 3–4). Slides were matched in the anterior–posterior plane. All analyzed slides were sliced 5 μm thick from 1 mm anterior to the bregma to 2 mm posterior to the bregma.

Two masked investigators carried out all analyses. For all assessed outcomes (cell counts and immunofluorescence), one slide per animal was quantified. For iNOS and 4-HNE immunofluorescence, four fields in total at 400× were analyzed per slide (two in the corpus callosum and two in the cortex). In the medial corpus callosum, two fields (right and left) were analyzed and their results were averaged. The area of each field was 150,000 μm^2 (450 μm width by 333 μm length). Similarly, in the frontal cerebral cortex, two fields (right and left) were analyzed and their results were averaged. The area of each field was 150,000 μm^2 (450 μm width by 333 μm length). Immunofluorescence analyses used NIH Image J software. Background was subtracted using the "Subtract Background" function on Image J.

Reviewers quantified NeuN positive cell count in the frontal cerebral cortex (layers 3–4, in the approximate watershed region where the anterior cerebral artery and middle cerebral artery converge) and Olig2 positive cell count in the corpus callosum using NIH image J software. Images were converted to 8-bit and adjusted to threshold to quantify cell counts.

TUNEL and NeuN double-positive cell counts were quantified in frontal cerebral cortical layers 3–4 to measure neuronal apoptosis. Two fields at 400× were analyzed per slide—one in the right and one in the left frontal cerebral cortex—and their results were averaged. The area of each field was .15 mm^2 (.45 mm width by .33 mm length). TUNEL and Olig2 double-positive cell counts were measured in the medial corpus callosum to quantify oligodendrocyte apoptosis. Two fields were analyzed per slide—one in the right and one in the left medial corpus callosum—and their results were averaged. The area of each field was .15 mm^2 (.45 mm width by .33 mm length). One slide for each animal was analyzed for TUNEL and cell counts analyses. Two independent, masked reviewers used NIH Image J software to quantify NeuN+TUNEL and Olig2 + TUNEL double-positive cell counts. All protocols adhered to the NIH Image J user guide.

The percent of cortical neuronal apoptosis was calculated by dividing the number of TUNEL and NeuN double-positive cells by the total number of NeuN positive cells. The percent of oligodendrocyte apoptosis in the corpus callosum was calculated by dividing the number of TUNEL and Olig2 double-positive cells by the total number of Olig2 positive cells.

2.9 | Statistical analysis

The Shapiro–Wilk test was performed to test for normality. All data sets were normally distributed. Two-way ANOVAs were used to analyze the effects of nPM and BCAS on study endpoints.
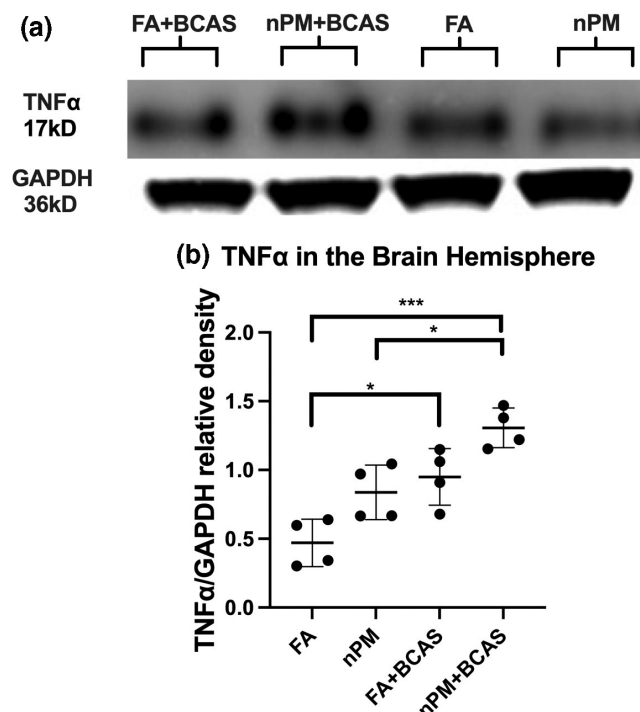
FIGURE 1 nPM and BCAS exposure caused increased TNFα protein in the brain hemisphere. (a) Representative western blots of brain hemisphere TNFα and GAPDH of each experimental group. (b) TNFα was increased in nPM+BCAS above filtered air (FA) ($p < .001$) and nPM ($p = .016$); and in FA+BCAS ($p = .013$) above FA. Data were analyzed using two-way ANOVAs. In the simple main effects model, nPM ($p = .001$) and BCAS ($p < .001$) had significant effects on TNFα levels in the brain hemisphere. Pairwise comparisons used Tukey's multiple comparisons test. Results from Tukey's multiple comparisons test are displayed on the graph. This exposure used nPM batch 5 (Table 2). Data represented as mean ± standard deviation. $n = 4$/group. *$p < .05$, **$p < .01$, ***$p < .001$.

Pairwise comparisons used Tukey's multiple comparisons test. For Olig2+CNPase and Olig2+PDGFRα double immunostaining, differences between FA and nPM groups were assessed using two-tailed unpaired student's *t* tests. Analyses were performed with GraphPad Prism software. Data are represented as mean ± standard deviation. Alpha level of .05 is considered statistically significant.

3 | RESULTS

3.1 | Cerebral blood flow (CBF) and mortality

Due to the resources and time needed to conduct FA/nPM exposures, this study (40 mice) was conducted as part of a larger cohort ($n = 108$). The additional mice ($n = 50$) were used in a different study and were never intended to be included in this study. However, total mortality was calculated using the larger cohort in an effort to be as transparent as possible. Mean cerebral blood flow (CBF) decrease after BCAS surgery was similar between FA+BCAS (42%) and nPM+BCAS groups (39.4%, $p = .634$). Eighteen mice died (16.7%) perioperatively and were excluded from analysis. Mortality occurred only in the FA+BCAS and nPM+BCAS groups. Total mortality in the BCAS groups was 31.6%. Mortality rates were equivalent among FA+BCAS (34.5%) and nPM+BCAS groups (28.6%, $p = .777$).
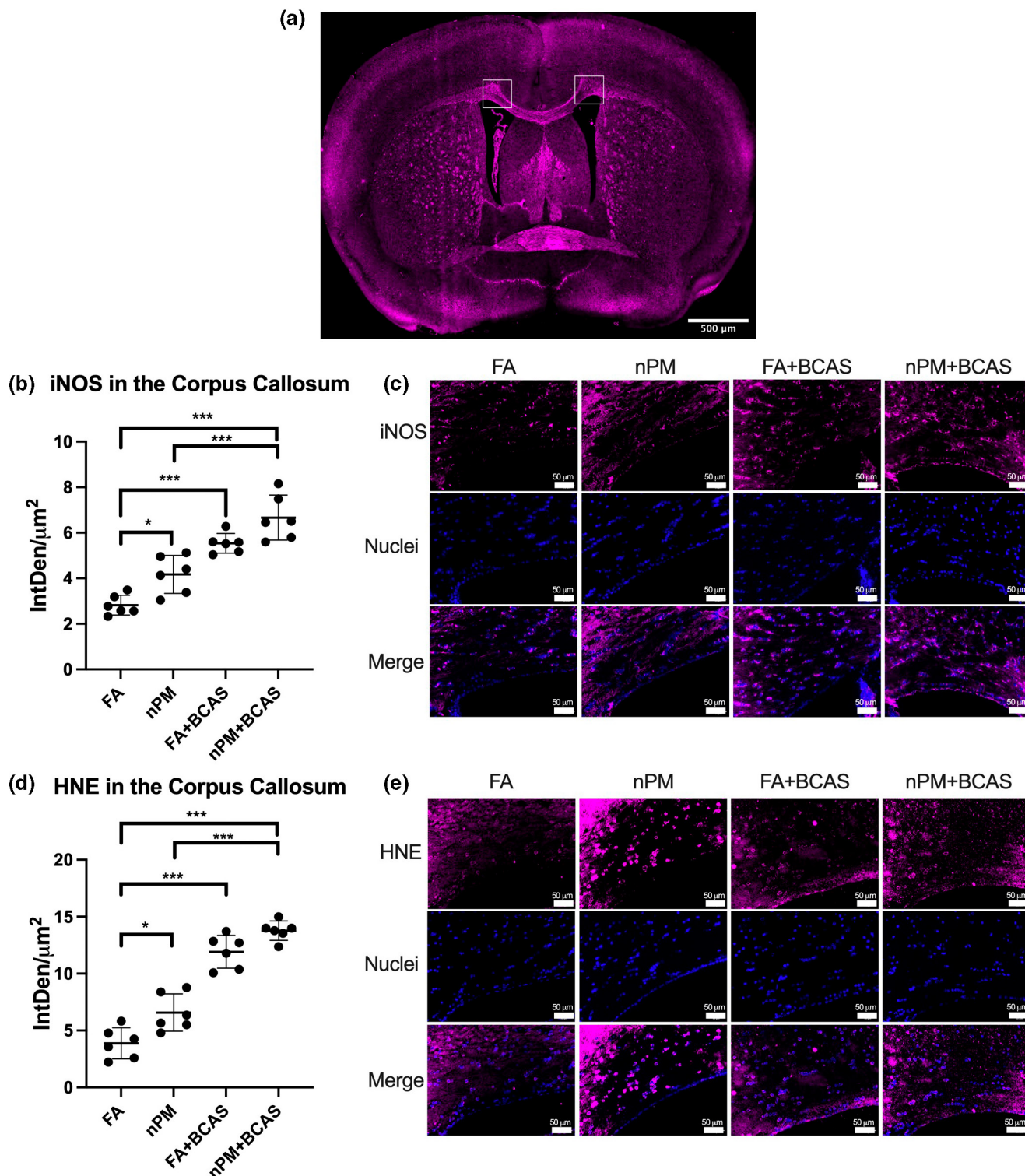
3.2 | Inflammation in the brain hemisphere

There was not a significant interaction between the effects of nPM and BCAS on TNFα brain hemisphere levels ($F(1,12) = .003$, $p = .954$) (Figure 1). Simple main effects analyses demonstrated that nPM and BCAS independently had significant effects on TNFα levels in the brain hemisphere (nPM: $F(1,13) = 17.08$, $p = .001$; BCAS: $F(1,13) = 29.33$, $p < .001$) (Figures 1 and S1). TNFα density was increased in the brain hemisphere of mice exposed to nPM+BCAS ($1.306 \pm .144$, $n = 4$) compared to FA ($.471 \pm .173$, $n = 4$) ($p < .001$) and nPM ($.848 \pm .199$, $n = 4$) ($p = .016$) (Figure 1). TNFα density was increased in the brain hemisphere of FA+BCAS mice ($.950 \pm .206$, $n = 4$) compared to FA ($p = .013$) (Figure 1).

3.3 | Oxidative stress in the corpus callosum and cerebral cortex

There was not a significant interaction between the effects of nPM and BCAS on iNOS integrated density in the corpus callosum ($F(1,20) = .144$, $p = .709$) (Figure 2). Simple main effects analyses
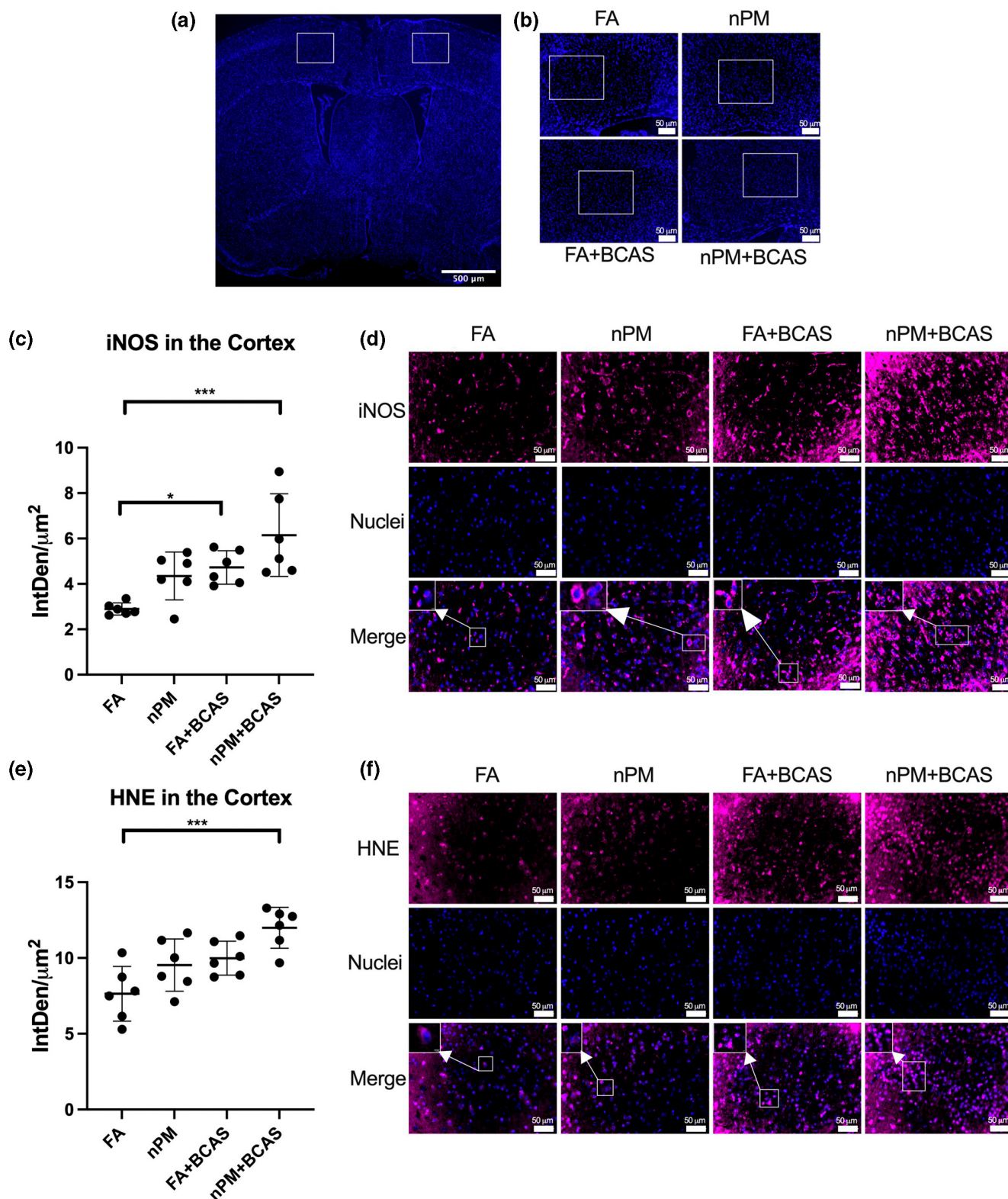
FIGURE 2 nPM and BCAS exposure caused increased oxidative stress in the corpus callosum. (a) Representative image of regions analyzed for all outcomes in the corpus callosum, including immunofluorescence and TUNEL/cell counting analyses. The right and left medial corpus callosum are demarcated as small boxes. Analyses include both right/left sides. Scale bar represents 500 μm. (b) iNOS integrated density in the corpus callosum was increased in nPM+BCAS compared to filtered air (FA) ($p < .001$) and nPM ($p < .001$); and in nPM ($p = .018$) and FA+BCAS ($p < .001$) compared to FA. In the simple main effects model, nPM ($p < .001$) and BCAS ($p < .001$) exposure had significant effects on iNOS integrated density in the corpus callosum. (c) Representative images of iNOS immunofluorescence (magenta) in the corpus callosum of each experimental group (400× magnification). Nuclei are stained with Hoechst 33342 (blue). Regions analyzed are demarcated in a. Scale bar represents 50 μm. (d) 4-HNE (HNE) integrated density was increased in the corpus callosum of nPM+BCAS compared to FA ($p < .001$) and nPM ($p < .001$); and in nPM ($p = .012$) and FA+BCAS ($p < .001$) compared to FA. In the simple main effects model, nPM ($p < .001$) and BCAS ($p < .001$) exposure had significant effects on 4-HNE integrated density in the corpus callosum. (e) Representative images of 4-HNE immunofluorescence (magenta) in the corpus callosum of each group (400× magnification). Nuclei are stained with Hoechst 33342 (blue). Regions analyzed are demarcated in a. Scale bar represents 50 μm. Data were analyzed using two-way ANOVAs. Pairwise comparisons used Tukey's multiple comparisons test. Results from Tukey's multiple comparisons test are displayed on the graphs. This exposure used nPM batches 1 and 2 (Table 2). Data represented as mean ± standard deviation. $n = 6$/group. *$p < .05$, **$p < .01$, ***$p < .001$.

(a)

(b) iNOS in the Corpus Callosum

(c)

(d) HNE in the Corpus Callosum

(e)

demonstrated that nPM and BCAS exposure independently had significant effects on iNOS integrated density in the corpus callosum (nPM: $F(1,21) = 18.9$, $p < .001$; BCAS: $F(1,21) = 83.11$, $p < .001$) (Figure 2). Combined nPM and BCAS exposure ($6.7 \pm .99$, $n = 6$) increased iNOS integrated density in the corpus callosum compared to FA ($2.8 \pm .43$, $n = 6$) ($p < .001$) and nPM ($4.2 \pm .83$, $n = 6$) ($p < .001$) exposures (Figure 2). iNOS integrated density was increased in the corpus callosum of mice exposed to nPM relative to FA ($p = .018$)

(Figure 2). iNOS integrated density was increased in the corpus callosum of the FA+BCAS group ($5.5 \pm .43$, $n = 6$) relative to FA ($p < .001$) (Figure 2).

There was not a significant interaction between the effects of nPM and BCAS on 4-HNE integrated density in the corpus callosum ($F(1,20) = .580$, $p = .455$) (Figure 2). Simple main effects analyses demonstrated that nPM and BCAS exposure independently had significant effects on 4-HNE integrated density in the corpus callosum

(a) (b) FA nPM FA+BCAS nPM+BCAS

(c) **iNOS in the Cortex** (d) FA nPM FA+BCAS nPM+BCAS

(e) **HNE in the Cortex** (f) FA nPM FA+BCAS nPM+BCAS

(nPM: $F(1,21) = 17.45$, $p < .001$; BCAS: $F(1,21) = 193.9$, $p < .001$) (Figure 2). 4-HNE integrated density was increased in the corpus callosum of mice exposed to nPM + BCAS ($13.8 \pm .85$, $n = 6$) relative to FA (3.9 ± 1.4, $n = 6$) ($p < .001$) and nPM (6.6 ± 1.6, $n = 6$) ($p < .001$) (Figure 2). 4-HNE integrated density was increased in the corpus callosum of mice exposed to nPM when compared to mice exposed to FA ($p = .012$). 4-HNE integrated density in the corpus callosum was increased in the FA + BCAS group (11.9 ± 1.5, $n = 6$) relative to FA ($p < .001$) (Figure 2).

There was not a significant interaction between the effects of nPM and BCAS on iNOS integrated density in the cortex ($F(1,20) = .001$, $p = .974$) (Figure 3). Simple main effects analyses demonstrated that nPM and BCAS exposure independently had significant effects on iNOS integrated density in the cortex (nPM:

JOURNAL OF

$F(1,21) = 10.34$, $p = .004$; BCAS: $F(1,21) = 16.51$, $p < .001$) (nPM: 4.3 ± 1.05, $n = 6$; BCAS: 4.7 ± .74, $n = 6$) (Figure 3). iNOS integrated density in the cortex was increased in mice exposed to nPM + BCAS (6.1 ± 1.82, $n = 6$) compared to mice exposed to FA (2.9 ± .27, $n = 6$) ($p < .001$) (Figure 3). iNOS integrated density was increased in FA + BCAS mice relative to FA ($p = .0472$) (Figure 3).

There was not a significant interaction between the effects of nPM and BCAS on 4-HNE integrated density in the cortex ($F(1,20) = .009$, $p = .928$) (Figure 3). Simple main effects analyses demonstrated that nPM and BCAS exposure independently had significant effects on 4-HNE integrated density in the cortex (nPM: $F(1,21) = 10.25$, $p = .004$; BCAS: $F(1,21) = 15.57$, $p < .001$) (nPM: 9.53 ± 1.73, $n = 6$; BCAS: 9.99 ± 1.12, $n = 6$) (Figure 3). nPM + BCAS exposure (12.0 ± 1.4, $n = 6$) increased 4-HNE integrated density in the cortex of mice when compared to FA (7.6 ± 1.8, $n = 6$) ($p < .001$) (Figure 3).

3.4 | Oligodendrocyte cell death in the corpus callosum

There was not a significant interaction between the effects of nPM and BCAS on oligodendrocyte cell counts in the corpus callosum ($F(1, 20) = .224$, $p = .641$) (Figure 4). Simple main effects analyses demonstrated that nPM and BCAS exposure independently had significant effects on oligodendrocyte cell counts in the corpus callosum (nPM: $F(1,21) = 15.64$, $p < .001$; BCAS: $F(1,21) = 17.25$, $p < .001$) (Figure 4). In the corpus callosum, mice exposed to nPM + BCAS (1150 ± 318, $n = 6$) had significantly decreased oligodendrocyte cell counts relative to FA (2280 ± 564, $n = 6$) ($p < .001$) (Figure 4). nPM exposure (1660 ± 168, $n = 6$) decreased oligodendrocyte cell counts in the corpus callosum relative to FA ($p = .028$). Oligodendrocyte cell counts in the corpus callosum were decreased in the FA + BCAS group (1630 ± 203, $n = 6$) when compared to FA controls ($p = .021$) (Figure 4).

There was not a significant interaction between the effects of nPM and BCAS on the percent of oligodendrocyte apoptosis in the corpus callosum ($F(1, 20) = 1.70$, $p = .207$) (Figure 4). Simple main effects analyses demonstrated that nPM and BCAS exposure independently had significant effects on the percent of oligodendrocyte apoptosis in the corpus callosum (nPM: $F(1,21) = 17.53$, $p < .001$; BCAS: $F(1,21) = 25.93$, $p < .001$) (Figure 4). Joint nPM and BCAS exposure increased the percentage of oligodendrocyte apoptosis (17.7 ± 7.4, $n = 6$) in the corpus callosum when compared to FA exposure (2.2 ± .78, $n = 6$) ($p < .001$) (Figure 4). nPM + BCAS exposure increased the percentage of oligodendrocyte apoptosis when compared to nPM (7.04 ± 1.86, $n = 6$) ($p = .001$) and FA + BCAS exposures (8.56 ± 2.47, $n = 6$) ($p = .004$) (Figure 4).

3.5 | Neuronal cell death in the cerebral cortex

There was not a significant interaction between the effects of nPM and BCAS on neuronal cell counts in the cerebral cortex ($F(1,20) = .597$, $p = .449$) (Figure 5). Simple main effects analyses demonstrated that nPM exposure did not have a significant effect on cortical neuronal cell counts ($F(1,21) = .710$, $p = .409$); however, BCAS exposure did have an effect on cortical neuronal cell counts ($F(1,21) = 41.57$, $p < .001$) (Figure 5). Neuronal cell counts in frontal cortical layers 3–4 were decreased in the nPM + BCAS group (924 ± 99.4, $n = 6$) compared to the FA (1610 ± 276, $n = 6$) ($p < .001$) and nPM (1600 ± 307, $n = 6$) ($p < .001$) groups (Figure 5). Cortical neuronal cell counts in frontal cerebral cortical layers 3–4 were decreased in the FA + BCAS group (1080 ± 179, $n = 6$) when compared to FA controls ($p = .004$) (Figure 5).

There was a significant interaction between the effects of nPM and BCAS on neuronal apoptosis in the cerebral cortex ($F(1,20) = 9.142$, $p = .007$) (Figure 5). Simple main effects analyses demonstrated that nPM and BCAS exposure independently had significant effects on the percent of neuronal apoptosis in the cortex (nPM: $F(1,21) = 7.08$, $p = .015$; BCAS: $F(1,21) = 31.61$, $p < .001$) (Figure 5). Frontal cortical neuronal apoptosis in layers 3–4 was increased in nPM + BCAS exposed mice (44.75 ± 9.1, $n = 6$) when compared to FA exposed mice (14.45 ± 8.2, $n = 6$) ($p < .001$) (Figure 5). nPM + BCAS exposure increased frontal cortical neuronal apoptosis in layers 3–4 when compared to nPM (14.79 ± 6.25, $n = 6$) ($p < .001$) and FA + BCAS exposure groups (25.62 ± 6.44, $n = 6$) ($p = .002$), respectively (Figure 5).
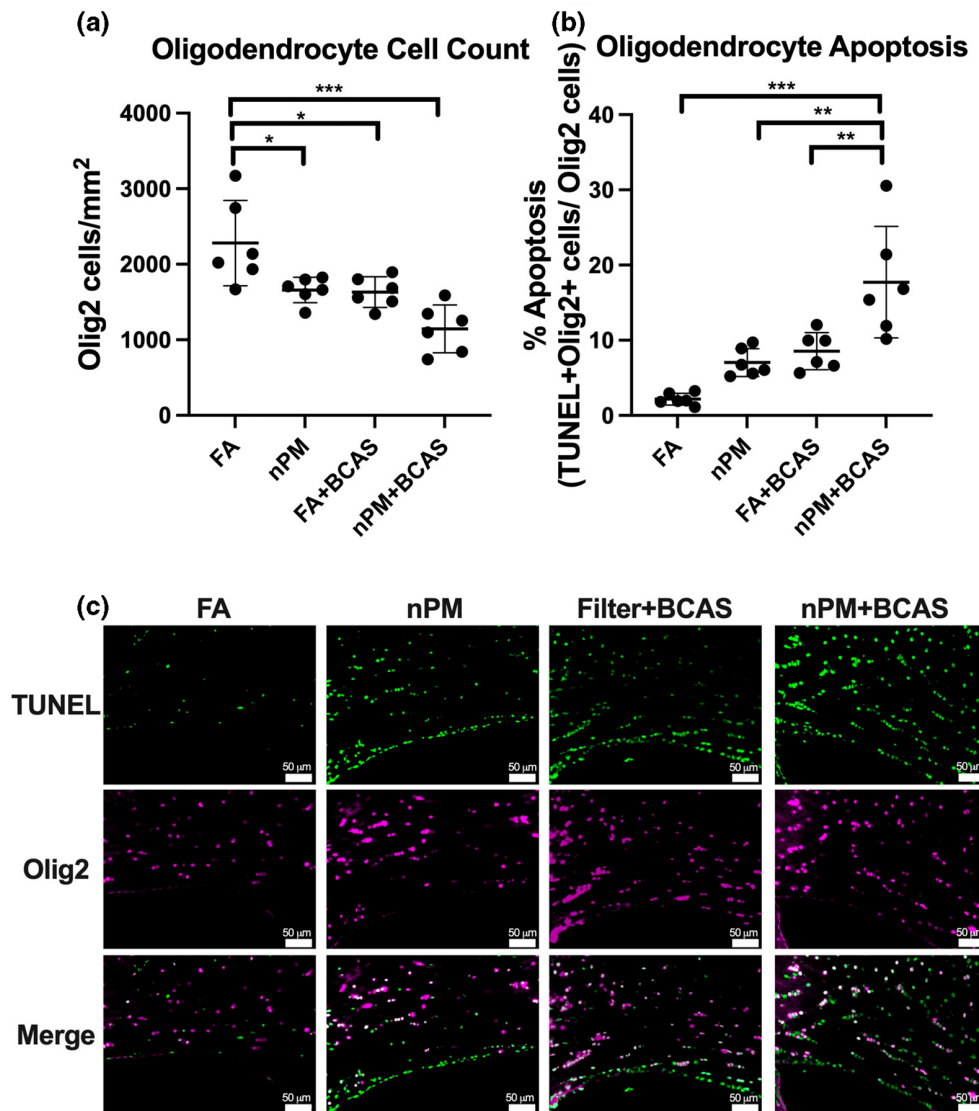
FIGURE 4 nPM and BCAS exposure caused oligodendrocyte cell death and apoptosis in the corpus callosum. (a) Oligodendrocyte cell counts in the corpus callosum were decreased in nPM+BCAS compared to FA ($p < .001$); and in nPM ($p = .028$) and FA+BCAS ($p = .021$) compared to FA. In the simple main effects model, nPM ($p < .001$) and BCAS ($p < .001$) had significant effects on oligodendrocyte cell counts in the corpus callosum. (b) Percentage of oligodendrocyte apoptosis in the corpus callosum was increased in nPM+BCAS compared to filtered air (FA) ($p < .001$), nPM ($p = .001$), and FA+BCAS ($p = .004$). In the simple main effects model, nPM ($p < .001$) and BCAS ($p < .001$) had significant effects on the percent of oligodendrocyte apoptosis in the corpus callosum. (c) Representative images of TUNEL (green) and Olig2 (magenta) double immunofluorescent staining in the corpus callosum of each experimental group. Regions analyzed are demarcated in Figure 2a. Scale bar represents 50 μm. Data were analyzed using two-way ANOVAs. Pairwise comparisons used Tukey's multiple comparisons test. Results from Tukey's multiple comparisons test are displayed on the graphs. This exposure used nPM batches 1 and 2 (Table 2). Data represented as mean ± standard deviation. $n = 6$/group. *$p < .05$, **$p < .01$, ***$p < .001$.

3.6 | Oligodendrocyte precursor cells (OPCs) and mature oligodendrocytes (mOLs) in the corpus callosum

As the above results demonstrated that nPM exposure increased total oligodendrocyte (and not neuronal) cell loss, this study investigated the response of OPCs and mOLs to nPM exposure. nPM exposure increased Olig2 and PDGFRα double-positive OPC cell counts (87 ± 12, $n = 10$) in the corpus callosum relative to FA (72 ± 21, $n = 12$) ($p = .048$) (Figure 6). nPM exposure decreased Olig2 and CNPase

double-positive mOL cell counts (420 ± 71, $n = 12$) in the corpus callosum relative to FA (602 ± 123, $n = 12$) ($p < .001$) (Figure 6).

4 | DISCUSSION

In the current study, combined nPM+BCAS exposure resulted in neuroinflammation (increased TNFα density) and oxidative stress (increased iNOS, 4HNE density) that was associated with oligodendrocyte and neuronal cell loss and apoptosis. The nPM exposure alone
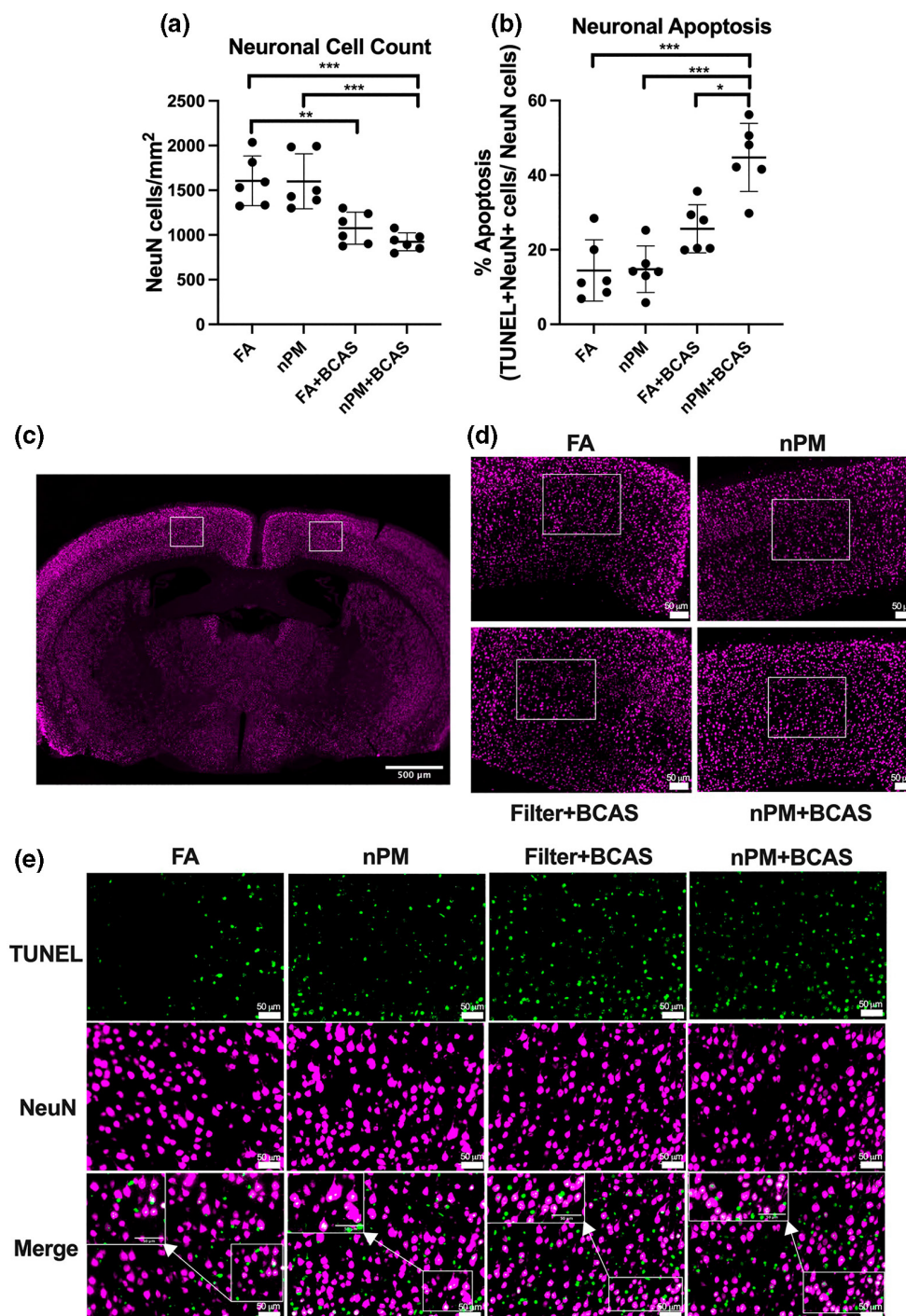
FIGURE 5 nPM and BCAS exposure caused neuronal cell death and apoptosis in the cerebral cortex. (a) Neuronal cell counts in the frontal cortex were decreased in nPM+BCAS compared to FA ($p < .001$) and nPM ($p < .001$); and in FA+BCAS compared to FA ($p = .004$). In the simple main effects model, nPM did not have an effect on cortical neuronal cell counts ($p = .409$), but BCAS did have a significant effect on cortical neuronal cell counts ($p < .001$). (b) nPM+BCAS exhibited a supra-additive effect on neuronal apoptosis ($p = .007$). Percentage of neuronal apoptosis in the frontal cortex was increased in nPM+BCAS compared to FA ($p < .001$), nPM ($p < .001$), and FA+BCAS ($p = .002$). In the simple main effects model, nPM ($p = .015$) and BCAS ($p < .001$) had significant effects on the percent of neuronal apoptosis in the cortex. (c) Low magnification (10×) image of regions analyzed. One section from both the right and left cortex was analyzed per mouse and their results were averaged. Scale bar represents 500 μm. (d) Lower magnification images of regions analyzed in each experimental group (200× magnification). Boxes denote the regions that were analyzed at 400× magnification. Scale bar represents 50 μm. (e) Representative images of TUNEL (green) and NeuN (magenta) double immunofluorescent staining in the cortex of each experimental group (400× magnification). Scale bar represents 50 μm. Data were analyzed using two-way ANOVAs. Pairwise comparisons used Tukey's multiple comparisons test. Results from Tukey's multiple comparisons test are displayed on the graphs. This exposure used nPM batches 1 and 2 (Table 2). Data represented as mean ± standard deviation. $n = 6$/group. *$p < .05$, **$p < .01$, ***$p < .001$.
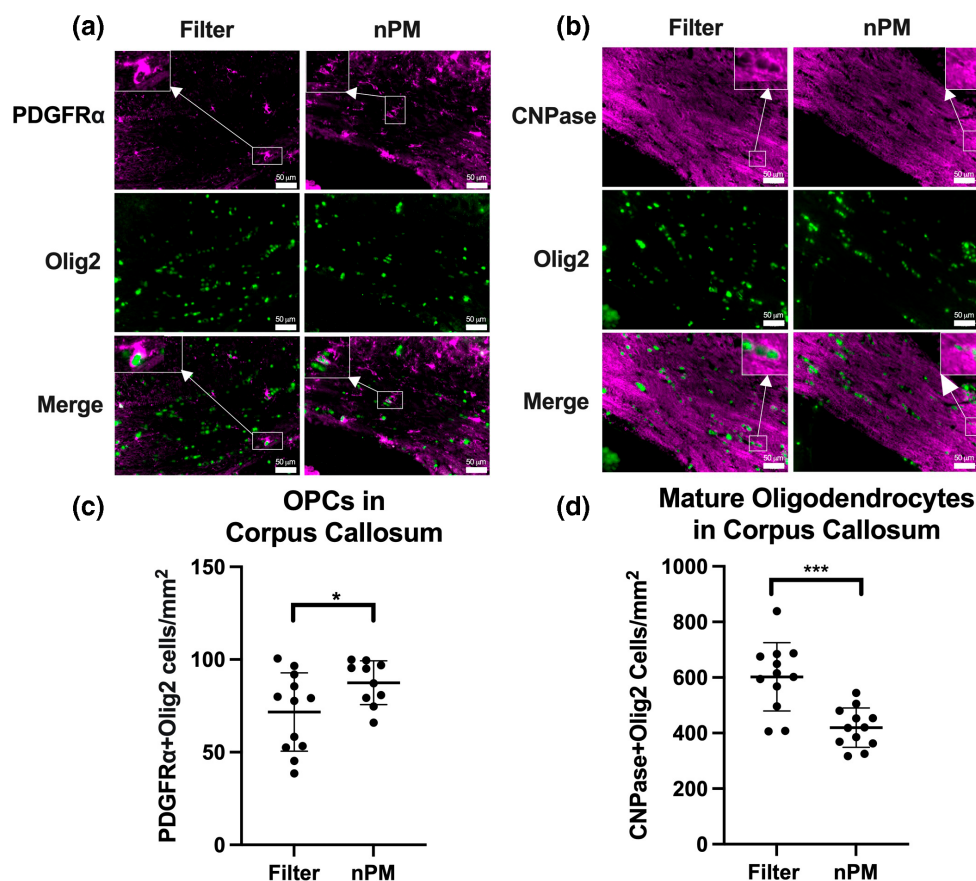
FIGURE 6 nPM exposure increases oligodendrocyte precursor cell (OPC) count and decreases mature oligodendrocyte (mOL) cell count in the corpus callosum. (a) Representative images of PDGFRα (magenta) and Olig2 (green) double immunofluorescent staining in the corpus callosum of each experimental group. Regions analyzed are demarcated in Figure 2a. Scale bar represents 50 μm. (b) Representative images of CNPase (magenta) and Olig2 (green) double immunofluorescent staining in the corpus callosum of each experimental group. Regions analyzed are demarcated in Figure 2a. Scale bar represents 50 μm. (c) nPM exposure increased oligodendrocyte precursor cells (OPCs) in the corpus callosum compared to FA ($p < .05$). $n = 10$ for nPM, 12 for FA. (d) nPM exposure decreased mature oligodendrocytes in the corpus callosum compared to FA ($p < .001$) $n = 12$/group. This exposure used nPM batches 1 and 2 (Table 2). Two-tailed unpaired student's t tests were used to analyze the data. Data represented as mean ± standard deviation. $*p < .05$, $**p < .01$, $***p < .001$.

caused total oligodendrocyte cell loss but did not cause neuronal cell loss. In particular, nPM exposure caused mature oligodendrocyte cell loss and increased OPC cell count. Joint nPM and BCAS exhibited a novel supra-additive effect on neuronal apoptosis. However, the combined effect of nPM and BCAS induced a greater increase in oligodendrocyte apoptosis than neuronal apoptosis when compared to FA (700% vs. 200% increase). These data confirm and extend prior studies that demonstrated white matter damage secondary to nPM and increased effects of combined nPM + BCAS exposure on corpus callosum white matter injury (Connor et al., 2021; Liu et al., 2021).

4.1 | Inflammation and oxidative stress: TNFα signaling and iNOS expression

Particulate matter and cerebral ischemia each trigger potent inflammation, which likely contributes to their respective neurotoxicities. The present study demonstrated increased TNFα protein in mouse brain hemisphere samples in the joint nPM + BCAS group. These

findings are consistent with prior experimental studies that establish that nPM exposure increases TNFα production in the systemic circulation and multiple brain regions (Babadjouni et al., 2018; Cheng, Davis, et al., 2016; Woodward, Levine, et al., 2017). Our previous murine experiments demonstrated that joint nPM + BCAS exposure increased whole brain TLR4 protein expression (Liu et al., 2021). Activation of the TLR4 pathway generates TNFα in-vitro and in-vivo (Woodward, Levine, et al., 2017; Zhang et al., 2007), which can increase blood–brain barrier permeability (BBB) and inhibit neurite outgrowth (Adivi et al., 2021; Cheng, Davis, et al., 2016; Nishioku et al., 2010). TNFα induces the NF-kB signaling pathway and may upregulate iNOS expression in glial cells and further activate inflammatory processes (Hayden & Ghosh, 2014; Saha & Pahan, 2006).

iNOS is expressed in neurons, microglia, astrocytes, and endothelial cells (Heneka & Feinstein, 2001; Sonar & Lal, 2019). Activated microglia upregulate iNOS and produce both NO and reactive oxygen species (ROS) (Kawabori & Yenari, 2015). Microglial activation has been previously demonstrated in the setting of nPM, BCAS, and joint nPM + BCAS exposures (Babadjouni et al., 2018; Connor

et al., 2021; Liu et al., 2021). The current study demonstrates increased iNOS staining in the corpus callosum in each of these exposure groups (nPM, BCAS, and joint nPM + BCAS). This increase may result in part from microglial activation. Similar results have been noted in human studies, with increased iNOS-positive cells in the cortex and olfactory bulb of individuals residing in a heavily polluted Mexican city compared to individuals residing in a less polluted city (Calderon-Garciduenas et al., 2008). Furthermore, iNOS may contribute to ischemia-associated neurotoxicity, as an experimental stroke study demonstrated smaller infarct volumes in iNOS knockout mice (Garry et al., 2015; Iadecola et al., 1997).

4.2 | Lipid oxidation

The interaction between excess NO and ROS can, in turn, produce peroxynitrite, a potent oxidant (Garcia-Bonilla et al., 2014; Garry et al., 2015; Koppal et al., 1999; Li et al., 2005). Chronic increases in NO and other oxidative stressors may result in lipid peroxidation, DNA/RNA damage, and protein oxidation/nitration (Liguori et al., 2018). A byproduct of lipid peroxidation, 4-HNE (HNE) induces neurotoxicity and may alter cell function by forming adducts with cysteine, lysine, or histidine residues of certain proteins (Breitzig et al., 2016; Di Domenico et al., 2017; Poli & Schaur, 2000). Furthermore, 4-HNE can activate macrophage scavenger receptors, causing macrophage/microglial activation. This may further propagate the inflammation and oxidative stress responses resulting from nPM and CCH exposure (Cheng, Saffari, et al., 2016; Ishii et al., 2004; Stewart et al., 2010).

The present study demonstrated increased 4-HNE production in the corpus callosum and cortex following combined nPM + BCAS exposure. These results are consistent with previous reports on the effects of ischemia and nPM in different brain regions. 4-HNE protein was increased in the ischemic penumbra of rats following middle cerebral artery occlusion (Li et al., 2018). Chronic nPM exposure (150 h total) increased 4-HNE, as well as APP and Aß levels in the cerebral cortex in J29-hAPPswe mice (Cacciottolo et al., 2020). In contrast, 45 h of nPM exposure in C57BL/6J mice increased 4-HNE levels in the olfactory bulb but not the cortex (Cheng, Saffari, et al., 2016). In a prolonged exposure to particulate matter (6 h/day, 5 days/week, for 9 months) levels of iNOS and HNE did not increase in the temporal cortex of mice (Bhatt et al., 2015). While a longer exposure period was utilized in the Bhatt et al. study, the particulate concentrations were lower than those in the present experiments (65.7 ± 34.2 vs. $330 \pm 25 \mu g/m^3$) (Bhatt et al., 2015). These results suggest that nPM exposure may induce oxidative stress in a tissue specific and dose-dependent manner.

4.3 | Apoptotic pathways

Our results suggest a role for apoptotic mechanisms in nPM and BCAS-induced neuronal and oligodendrocyte toxicity. Intrinsic and extrinsic apoptotic pathways can be induced in response to 4-HNE. (McCracken et al., 2000; Zhang et al., 2017). Furthermore, TNFα can directly induce the extrinsic apoptosis pathway through its receptors TNFR1/2 (Bertheloot et al., 2021).

The current investigation demonstrated that combined nPM + BCAS exposure increased oligodendrocyte and neuronal cell death via apoptotic pathways. Interestingly, nPM exposure alone did not decrease cortical neuronal cell counts but did decrease oligodendrocyte cell counts in the corpus callosum.

4.4 | Combined effects of nPM and CCH

There was a significant interaction between nPM and BCAS on neuronal TUNEL staining (combined effect was 2.6× the additive effects of nPM and BCAS). This may suggest a supra-additive interaction between an environmental exposure and underlying cerebrovascular disease. This interaction may be influenced by the lack of effect of nPM exposure on neuronal TUNEL staining. There was not a significant interaction between nPM and BCAS on oligodendrocyte TUNEL staining. However, cortical neuronal TUNEL staining increased by 200% and corpus callosum oligodendrocyte TUNEL staining increased by 700% in the nPM + BCAS group when compared to filtered air controls. These results suggest a greater effect of nPM and joint nPM + BCAS exposures on oligodendrocytes and white matter.

4.5 | Effects of nPM and CCH on oligodendrocytes and white matter

White matter may be preferentially vulnerable to neurotoxicity following PM and CCH exposures (Babadjouni et al., 2018; Calderón-Garcidueñas et al., 2008; Chen et al., 2015, 2020; Kim, Kim, et al., 2020; Woodward, Pakbin, et al., 2017). In the Women's Health Initiative Memory Study, increased $PM_{2.5}$ exposure was associated with decreased white matter volumes but unchanged gray matter volumes in older women. Stronger associations between white matter volumes and $PM_{2.5}$ exposure were noted in women with prior cerebrovascular disease (Chen et al., 2015). These results suggest potentially interrelated mechanisms underlying nPM- and ischemia-induced white matter toxicity.

Previous experimental and epidemiological investigations have demonstrated white matter injury following nPM exposure (Allen et al., 2017; Calderón-Garcidueñas et al., 2011; Calderón-Garcidueñas et al., 2008; Casanova et al., 2016; Chen et al., 2015; Connor et al., 2021; Erickson et al., 2020; Liu et al., 2021; Woodward, Pakbin, et al., 2017). Our prior murine studies have demonstrated that chronic nPM exposure (150 h) can induce myelin injury and total oligodendrocyte cell death in the corpus callosum (Connor et al., 2021; Liu et al., 2021). The damage was exacerbated by BCAS in a supra-additive manner (Liu et al., 2021). Furthermore, myelin injury has been noted in the CA1 stratum

oriens region of the hippocampus in young mice exposed to nPM (Woodward, Pakbin, et al., 2017). Human studies have demonstrated similar results. Children residing in a highly polluted Mexican city had greater prefrontal white injury and cognitive deficits than those residing in a less polluted area (Calderón-Garcidueñas et al., 2008, 2011).

4.6 | Effects of nPM and CCH on neurons and gray matter

In the present study, nPM exposure induced neuronal TUNEL staining in the frontal cerebral cortex (layers 3–4) only in the setting of BCAS. Our laboratory has previously shown a temporal increase in BBB permeability secondary to decreased pericyte coverage in the murine BCAS model (Liu et al., 2019). BBB dysfunction occurs in advance of white matter damage (Liu et al., 2019). Likewise, transient BBB dysfunction may allow nPM-induced inflammation and oxidative stress products to cross from the systemic vasculature into the cerebral cortex and promote neuronal cell death or exacerbate white matter injury.

Frontal cortical neurons in layers 3–4 were examined in this study, similar to a prior study which quantified levels of HNE in cortical neurons in layers 2–4 after nPM exposure (Cacciottolo et al., 2020). Pyramidal neurons in layer 3 are uniquely susceptible to ischemia (Baron et al., 2014). Neurons in layer 4 are important in information processing and are prone to anoxic depolarization, a hallmark of ischemic brain injury (Juzekaeva et al., 2017).

Prior reports have principally focused on the neurotoxic effect of developmental PM exposure on hippocampal and cortical neurons. Studies have demonstrated that gestational $PM_{2.5}$ exposure increased apoptosis of cerebral cortical neurons, as well as hippocampal neurons in mice (CA1, CA3, DG regions) (Zhang et al., 2018; Zheng et al., 2019). Outside of the developmental period, chronic nPM exposure in 3-month-old mice has been shown to induce neurite atrophy in the CA1 region of the hippocampus (Woodward, Pakbin, et al., 2017).

Neuronal damage has been noted in the hippocampus, cerebral cortex, and striatum following cerebral hypoperfusion. Poh et al. demonstrated neuronal loss with decreased MAP2 immunofluorescence in the cerebral cortex, hippocampus, and striatum at day 30 post-BCAS surgery in a murine model (Poh et al., 2020). Furthermore, markers of both apoptosis and pyroptosis were increased in the cerebral cortex and hippocampus of BCAS mice compared to sham mice (Poh et al., 2020).

4.7 | Effects of nPM on oligodendrocyte precursor cells and mature oligodendrocytes

Our results demonstrated that nPM exposure induced oligodendrocyte cell loss in the corpus callosum, without promoting cortical neuronal cell loss. Given these results, we sought to determine the response of oligodendrocyte precursor cells to nPM exposure. In response to injury, local OPCs and OPCs from the subventricular zone can proliferate, migrate to sites of injury, and differentiate into mOLs (Bergles & Richardson, 2015; Gallo & Armstrong, 2008). The decreased number of mature oligodendrocytes and increased number of OPCs in the corpus callosum following nPM exposure may represent an adaptive response to injury. The fact that the total number of oligodendrocytes is decreased may suggest deficiencies in oligodendrocyte differentiation, rather than migration or proliferation. Previous studies have suggested that OPCs may be preferentially susceptible to oxidative stress given their reduced antioxidant capacity when compared to mOLs (Kim, Kim, et al., 2020; Spaas et al., 2021). However, these cells also may exhibit rapid turnover. An in-vitro cell culture study demonstrated that ultrafine urban PM (uf-UP) exposure induced more severe injury in OPCs and mOLs compared to cortical neurons, with the greatest injury observed in OPCs. This cellular injury was associated with ROS induction and decreased antioxidant capacity (Kim, Kim, et al., 2020).

High levels of oxidative stress may induce OPC death, but sublethal levels can disrupt OPC differentiation (Lloret et al., 2021; Miyamoto et al., 2013; Spaas et al., 2021). In-vitro, ROS exposure altered the expression of oligodendrocyte differentiation regulators, increasing the expression of inhibitors and reducing the expression of positive regulators (French et al., 2009; Lim et al., 2016; Spaas et al., 2021).

In the present study, nPM exposure induced mOL cell death and increased OPC cell number. Overall, total oligodendrocytes were decreased following nPM exposure. These results suggest that nPM exposure may induce a maturation block, potentially inhibiting the differentiation of OPCs into mOLs. The increased cell number of OPCs may be secondary to the proliferation of local OPCs or the migration of OPCs from nearby sites or the subventricular zone. Similarly, in a murine model, white matter stroke induced local OPCs proliferation in the peri-infarct area; however, these OPCs failed to differentiate into mOLs (Sozmen et al., 2016). Ischemia has also been shown to induce oxidative stress, which in turns inhibits oligodendrocyte maturation. Edaravone, a radical scavenger, reduced oxidative stress markers and rescued OPC differentiation in mice exposed to CCH secondary to BCAS (Miyamoto et al., 2013). Disruption of oligodendrocyte differentiation underlies the pathogenesis of multiple neurological disorders, including Alzheimer's disease, multiple sclerosis, and Parkinson's disease (Spaas et al., 2021). The present study suggests that nPM exposure promotes oxidative stress, which may affect OPC dysfunction and the inhibition of oligodendrocyte differentiation.

4.8 | Strengths and limitations

There are several strengths and limitations of this study. Differences between exposures are reflective of the natural changes in Los Angeles aerosol since nPM batches were collected across different years and seasons. All nPM batches were collected from the same

location to minimize variability in nPM composition. The size distributions of the exposures were representative of PM in the Los Angeles air basin (Table 2) (Hudda et al., 2010; Taghvaee et al., 2019). Furthermore, mass fractions of organic carbon, trace elements, and metals in the current nPM batches were congruent with our prior studies in Los Angeles (Altuwayjiri et al., 2020; Hasheminassab, Daher, Saffari, et al., 2014; Saffari et al., 2013; Sardar et al., 2005; Shirmohammadi et al., 2016). This study was not designed to assess the dose-dependent effect of nPM exposure on oligodendrocyte and neuronal injury. While nPM exposure alone did not induce neuronal injury in this study, nPM exposure over a longer time period or at a higher concentration may promote neuronal degradation. Oxidative stress and apoptotic responses to independent nPM exposure likely vary depending on the year collected (Zhang et al., 2021). In this study, nPM exposure alone induced oxidative stress and oligodendrocyte cell loss in the corpus callosum. The effect of nPM exposure may be less robust when using more recent nPM batches collected from Los Angeles.

Due to sample size limitations, the experimental cohort consisted of male mice only and did not address sex differences. This is a significant limitation of the manuscript. Estrogen has been suggested to protect against neuronal and white matter injury (Allen et al., 2017; Brotfain et al., 2016; Dominguez et al., 2018). Future studies should assess the influence of sex on outcomes following nPM and BCAS exposure. The TUNEL assay used in this study stains for double-stranded DNA breaks, which can be produced during apoptosis. While TUNEL is a sensitive marker for apoptosis, TUNEL may stain cells with DNA damage that are not actively undergoing apoptosis (Mirzayans & Murray, 2020). Therefore, our results may marginally overestimate the percentage of apoptosis in oligodendrocytes and neurons (Kyrylkova et al., 2012). Sample sizes were small, which may have influenced outcomes. such as oligodendrocyte apoptosis, which did not demonstrate a significant interaction between nPM and BCAS. Findings should therefore be interrupted with caution given sample size restraints. While this study focuses on apoptosis, additional cell death pathways, such as pyroptosis and necroptosis, are likely activated following nPM and BCAS exposures. All outcome measures (TNFα, iNOS, HNE, etc.) in this investigation were assessed at a single time-point. The study was not designed to characterize the time-course by which nPM and BCAS exposures induce inflammatory and oxidative stress pathways that cause neuronal and white matter injury.

5 | CONCLUSIONS

Data from the current experiments indicate that exposure to nPM and BCAS promotes neuroinflammation and oxidative stress, which can induce neuronal and white matter damage via apoptotic pathways. Combined nPM and BCAS exposure exhibit increased effects on cortical neuronal injury. However, the present study suggests that oligodendrocytes in the corpus callosum are preferentially susceptible to the toxic effects of nPM and BCAS exposure. Specifically, nPM exposure causes cell death in mature oligodendrocytes but appears to increase the number of oligodendrocyte precursor cells. Vulnerable populations, such as those with underlying cerebrovascular disease, may be at greater risk for white matter injury secondary to air pollution exposure.

CONFLICT OF INTEREST

William J. Mack is a consultant for Rebound Therapeutics, Viseon, Imperative Care, Integra, Q'Apel, Stryker, Stream Biomedical, and Spartan Micro. William J. Mack is an investor for Cerebrotech, Endostream, Viseon, Rebound, Spartan Micro, Truvic, Imperative Care, and Q'Apel.

PEER REVIEW

The peer review history for this article is available at https://publons.com/publon/10.1002/jnr.25153.

DATA AVAILABILITY STATEMENT

All data in this study are available from the corresponding author on reasonable request.

ORCID

Brandon Ge https://orcid.org/0000-0002-8775-8521

REFERENCES

Adivi, A., Lucero, J., Simpson, N., McDonald, J. D., & Lund, A. K. (2021). Exposure to traffic-generated air pollution promotes alterations in the integrity of the brain microvasculature and inflammation in female ApoE(−/−) mice. *Toxicology Letters*, *339*, 39–50. https://doi.org/10.1016/j.toxlet.2020.12.016

Allen, J. L., Oberdorster, G., Morris-Schaffer, K., Wong, C., Klocke, C., Sobolewski, M., Conrad, K., Mayer-Proschel, M., & Cory-Slechta,

D. A. (2017). Developmental neurotoxicity of inhaled ambient ultrafine particle air pollution: Parallels with neuropathological and behavioral features of autism and other neurodevelopmental disorders. *Neurotoxicology*, *59*, 140–154. https://doi.org/10.1016/j.neuro.2015.12.014

Altuwayjiri, A., Pirhadi, M., Taghvaee, S., & Sioutas, C. (2020). Long-term trends in the contribution of PM(2.5) sources to organic carbon (OC) in the Los Angeles basin and the effect of PM emission regulations. *Faraday Discussions*, *226*, 74–99. https://doi.org/10.1039/d0fd00074d

Babadjouni, R., Patel, A., Liu, Q., Shkirkova, K., Lamorie-Foote, K., Connor, M., Hodis, D. M., Cheng, H., Sioutas, C., Morgan, T. E., Finch, C. E., & Mack, W. J. (2018). Nanoparticulate matter exposure results in neuroinflammatory changes in the corpus callosum. *PLoS One*, *13*(11), e0206934. https://doi.org/10.1371/journal.pone.0206934

Baron, J. C., Yamauchi, H., Fujioka, M., & Endres, M. (2014). Selective neuronal loss in ischemic stroke and cerebrovascular disease. *Journal of Cerebral Blood Flow and Metabolism*, *34*(1), 2–18. https://doi.org/10.1038/jcbfm.2013.188

Bergles, D. E., & Richardson, W. D. (2015). Oligodendrocyte development and plasticity. *Cold Spring Harbor Perspectives in Biology*, *8*(2), a020453. https://doi.org/10.1101/cshperspect.a020453

Bertheloot, D., Latz, E., & Franklin, B. S. (2021). Necroptosis, pyroptosis and apoptosis: An intricate game of cell death. *Cellular & Molecular Immunology*, *18*(5), 1106–1121. https://doi.org/10.1038/s41423-020-00630-3

Bhatt, D. P., Puig, K. L., Gorr, M. W., Wold, L. E., & Combs, C. K. (2015). A pilot study to assess effects of long-term inhalation of airborne particulate matter on early Alzheimer-like changes in the mouse brain. *PLoS One*, *10*(5), e0127102. https://doi.org/10.1371/journal.pone.0127102

Biran, R., Tang, Y.-Z., Brook, J., Vincent, R., & Keeler, G. (1996). Aqueous extraction of airborne particulate matter collected on hi-vol Teflon filters. *International Journal of Environmental Analytical Chemistry*, *63*(4), 315–322.

Block, M. L., Elder, A., Auten, R. L., Bilbo, S. D., Chen, H., Chen, J. C., Cory-Slechta, D. A., Costa, D., Diaz-Sanchez, D., Dorman, D. C., Gold, D. R., Gray, K., Jeng, H. A., Kaufman, J. D., Kleinman, M. T., Kirshner, A., Lawler, C., Miller, D. S., Nadadur, S. S., ... Wright, R. J. (2012). The outdoor air pollution and brain health workshop. *Neurotoxicology*, *33*(5), 972–984. https://doi.org/10.1016/j.neuro.2012.08.014

Breitzig, M., Bhimineni, C., Lockey, R., & Kolliputi, N. (2016). 4-Hydroxy-2-nonenal: A critical target in oxidative stress? *American Journal of Physiology. Cell Physiology*, *311*(4), C537–c543. https://doi.org/10.1152/ajpcell.00101.2016

Brotfain, E., Gruenbaum, S. E., Boyko, M., Kutz, R., Zlotnik, A., & Klein, M. (2016). Neuroprotection by estrogen and progesterone in traumatic brain injury and spinal cord injury. *Current Neuropharmacology*, *14*(6), 641–653. https://doi.org/10.2174/1570159x14666160309123554

Cacciottolo, M., Morgan, T. E., Saffari, A. A., Shirmohammadi, F., Forman, H. J., Sioutas, C., & Finch, C. E. (2020). Traffic-related air pollutants (TRAP-PM) promote neuronal amyloidogenesis through oxidative damage to lipid rafts. *Free Radical Biology & Medicine*, *147*, 242–251. https://doi.org/10.1016/j.freeradbiomed.2019.12.023

Cacciottolo, M., Wang, X., Driscoll, I., Woodward, N., Saffari, A., Reyes, J., Serre, M. L., Vizuete, W., Sioutas, C., Morgan, T. E., Gatz, M., Chui, H. C., Shumaker, S. A., Resnick, S. M., Espeland, M. A., Finch, C. E., & Chen, J. C. (2017). Particulate air pollutants, APOE alleles and their contributions to cognitive impairment in older women and to amyloidogenesis in experimental models. *Translational Psychiatry*, *7*(1), e1022. https://doi.org/10.1038/tp.2016.280

Calderón-Garcidueñas, L., Engle, R., Mora-Tiscareño, A., Styner, M., Gómez-Garza, G., Zhu, H., Jewells, V., Torres-Jardón, R., Romero, L., Monroy-Acosta, M. E., Bryant, C., González-González, L. O., Medina-Cortina, H., & D'Angiulli, A. (2011). Exposure to severe urban air pollution influences cognitive outcomes, brain volume and systemic inflammation in clinically healthy children. *Brain and Cognition*, *77*(3), 345–355. https://doi.org/10.1016/j.bandc.2011.09.006

Calderón-Garcidueñas, L., Mora-Tiscareño, A., Ontiveros, E., Gómez-Garza, G., Barragán-Mejía, G., Broadway, J., Chapman, S., Valencia-Salazar, G., Jewells, V., Maronpot, R. R., Henríquez-Roldán, C., Pérez-Guillé, B., Torres-Jardón, R., Herrit, L., Brooks, D., Osnaya-Brizuela, N., Monroy, M. E., González-Maciel, A., Reynoso-Robles, R., ... Engle, R. W. (2008). Air pollution, cognitive deficits and brain abnormalities: A pilot study with children and dogs. *Brain and Cognition*, *68*(2), 117–127. https://doi.org/10.1016/j.bandc.2008.04.008

Calderon-Garciduenas, L., Solt, A. C., Henriquez-Roldan, C., Torres-Jardon, R., Nuse, B., Herritt, L., Villarreal-Calderón, R., Osnaya, N., Stone, I., García, R., Brooks, D. M., González-Maciel, A., Reynoso-Robles, R., Delgado-Chávez, R., & Reed, W. (2008). Long-term air pollution exposure is associated with neuroinflammation, an altered innate immune response, disruption of the blood-brain barrier, ultrafine particulate deposition, and accumulation of amyloid beta-42 and alpha-synuclein in children and young adults. *Toxicologic Pathology*, *36*(2), 289–310. https://doi.org/10.1177/0192623307313011

Casanova, R., Wang, X., Reyes, J., Akita, Y., Serre, M. L., Vizuete, W., Chui, H. C., Driscoll, I., Resnick, S. M., Espeland, M. A., & Chen, J. C. (2016). A voxel-based morphometry study reveals local brain structural alterations associated with ambient Fine particles in older women. *Frontiers in Human Neuroscience*, *10*, 495. https://doi.org/10.3389/fnhum.2016.00495

Chen, C., Xun, P., Kaufman, J. D., Hayden, K. M., Espeland, M. A., Whitsel, E. A., Serre, M. L., Vizuete, W., Orchard, T., Harris, W. S., Wang, X., Chui, H. C., Chen, J. C., & He, K. (2020). Erythrocyte omega-3 index, ambient fine particle exposure, and brain aging. *Neurology*, *95*(8), e995–e1007. https://doi.org/10.1212/wnl.0000000000010074

Chen, H., Kwong, J. C., Copes, R., Tu, K., Villeneuve, P. J., van Donkelaar, A., Hystad, P., Martin, R. V., Murray, B. J., Jessiman, B., Wilton, A. S., Kopp, A., & Burnett, R. T. (2017). Living near major roads and the incidence of dementia, Parkinson's disease, and multiple sclerosis: A population-based cohort study. *Lancet*, *389*(10070), 718–726. https://doi.org/10.1016/s0140-6736(16)32399-6

Chen, J. C., Wang, X., Wellenius, G. A., Serre, M. L., Driscoll, I., Casanova, R., McArdle, J. J., Manson, J. E., Chui, H. C., & Espeland, M. A. (2015). Ambient air pollution and neurotoxicity on brain structure: Evidence from women's health initiative memory study. *Annals of Neurology*, *78*(3), 466–476. https://doi.org/10.1002/ana.24460

Cheng, H., Davis, D. A., Hasheminassab, S., Sioutas, C., Morgan, T. E., & Finch, C. E. (2016). Urban traffic-derived nanoparticulate matter reduces neurite outgrowth via TNFα in vitro. *Journal of Neuroinflammation*, *13*, 19. https://doi.org/10.1186/s12974-016-0480-3

Cheng, H., Saffari, A., Sioutas, C., Forman, H. J., Morgan, T. E., & Finch, C. E. (2016). Nanoscale particulate matter from urban traffic rapidly induces oxidative stress and inflammation in olfactory epithelium with concomitant effects on brain. *Environmental Health Perspectives*, *124*(10), 1537–1546. https://doi.org/10.1289/ehp134

Connor, M., Lamorie-Foote, K., Liu, Q., Shkirkova, K., Baertsch, H., Sioutas, C., Morgan, T. E., Finch, C. E., & Mack, W. J. (2021). Nanoparticulate matter exposure results in white matter damage and an inflammatory microglial response in an experimental murine model. *PLoS One*, *16*(7), e0253766. https://doi.org/10.1371/journal.pone.0253766

Crane, D. E., Black, S. E., Ganda, A., Mikulis, D. J., Nestor, S. M., Donahue, M. J., & MacIntosh, B. J. (2015). Gray matter blood flow and volume are reduced in association with white matter hyperintensity lesion burden: A cross-sectional MRI study. *Frontiers in Aging Neuroscience*, *7*, 131. https://doi.org/10.3389/fnagi.2015.00131

Dalleau, S., Baradat, M., Guéraud, F., & Huc, L. (2013). Cell death and diseases related to oxidative stress: 4-hydroxynonenal (HNE) in the balance. *Cell Death and Differentiation*, *20*(12), 1615–1630. https://doi.org/10.1038/cdd.2013.138

Di Domenico, F., Tramutola, A., & Butterfield, D. A. (2017). Role of 4-hydroxy-2-nonenal (HNE) in the pathogenesis of alzheimer disease and other selected age-related neurodegenerative disorders. *Free Radical Biology & Medicine*, *111*, 253–261. https://doi.org/10.1016/j.freeradbiomed.2016.10.490

Dominguez, R., Zitting, M., Liu, Q., Patel, A., Babadjouni, R., Hodis, D. M., Chow, R. H., & Mack, W. J. (2018). Estradiol protects white matter of male C57BL6J mice against experimental chronic cerebral hypoperfusion. *Journal of Stroke and Cerebrovascular Diseases*, *27*(7), 1743–1751. https://doi.org/10.1016/j.jstrokecerebrovasdis.2018.01.030

Erickson, L. D., Gale, S. D., Anderson, J. E., Brown, B. L., & Hedges, D. W. (2020). Association between exposure to air pollution and total gray matter and total white matter volumes in adults: A cross-sectional study. *Brain Sciences*, *10*(3), 164. https://doi.org/10.3390/brainsci10030164

French, H. M., Reid, M., Mamontov, P., Simmons, R. A., & Grinspan, J. B. (2009). Oxidative stress disrupts oligodendrocyte maturation. *Journal of Neuroscience Research*, *87*(14), 3076–3087. https://doi.org/10.1002/jnr.22139

Gallo, V., & Armstrong, R. C. (2008). Myelin repair strategies: A cellular view. *Current Opinion in Neurology*, *21*(3), 278–283. https://doi.org/10.1097/WCO.0b013e3282fd1875

Garcia-Bonilla, L., Moore, J. M., Racchumi, G., Zhou, P., Butler, J. M., Iadecola, C., & Anrather, J. (2014). Inducible nitric oxide synthase in neutrophils and endothelium contributes to ischemic brain injury in mice. *Journal of Immunology*, *193*(5), 2531–2537. https://doi.org/10.4049/jimmunol.1400918

Garry, P. S., Ezra, M., Rowland, M. J., Westbrook, J., & Pattinson, K. T. (2015). The role of the nitric oxide pathway in brain injury and its treatment—From bench to bedside. *Experimental Neurology*, *263*, 235–243. https://doi.org/10.1016/j.expneurol.2014.10.017

Giacci, M. K., Bartlett, C. A., Smith, N. M., Iyer, K. S., Toomey, L. M., Jiang, H., Guagliardo, P., Kilburn, M. R., & Fitzgerald, M. (2018). Oligodendroglia are particularly vulnerable to oxidative damage after neurotrauma in vivo. *The Journal of Neuroscience*, *38*(29), 6491–6504. https://doi.org/10.1523/jneurosci.1898-17.2018

Hasheminassab, S., Daher, N., Ostro, B. D., & Sioutas, C. (2014). Long-term source apportionment of ambient fine particulate matter (PM2. 5) in the Los Angeles Basin: A focus on emissions reduction from vehicular sources. *Environmental Pollution*, *193*, 54–64.

Hasheminassab, S., Daher, N., Saffari, A., Wang, D., Ostro, B. D., & Sioutas, C. (2014). Spatial and temporal variability of sources of ambient fine particulate matter ($PM_{2.5}$) in California. *Atmospheric Chemistry and Physics*, *14*(22), 12085–12097. https://doi.org/10.5194/acp-14-12085-2014

Hayden, M. S., & Ghosh, S. (2014). Regulation of NF-κB by TNF family cytokines. *Seminars in Immunology*, *26*(3), 253–266. https://doi.org/10.1016/j.smim.2014.05.004

Heneka, M. T., & Feinstein, D. L. (2001). Expression and function of inducible nitric oxide synthase in neurons. *Journal of Neuroimmunology*, *114*(1–2), 8–18.

Hudda, N., Cheung, K., Moore, K. F., & Sioutas, C. (2010). Inter-community variability in total particle number concentrations in the eastern Los Angeles air basin. *Atmospheric Chemistry and Physics*, *10*(23), 11385–11399. https://doi.org/10.5194/acp-10-11385-2010

Iadecola, C., Zhang, F., Casey, R., Nagayama, M., & Ross, M. E. (1997). Delayed reduction of ischemic brain injury and neurological deficits in mice lacking the inducible nitric oxide synthase gene. *The Journal of Neuroscience*, *17*(23), 9157–9164.

Ishii, T., Itoh, K., Ruiz, E., Leake, D. S., Unoki, H., Yamamoto, M., & Mann, G. E. (2004). Role of Nrf2 in the regulation of CD36 and stress protein expression in murine macrophages: Activation by oxidatively modified LDL and 4-hydroxynonenal. *Circulation Research*, *94*(5), 609–616. https://doi.org/10.1161/01.Res.0000119171.44657.45

Juzekaeva, E., Nasretdinov, A., Gainutdinov, A., Sintsov, M., Mukhtarov, M., & Khazipov, R. (2017). Preferential initiation and spread of anoxic depolarization in layer 4 of rat barrel cortex. *Frontiers in Cellular Neuroscience*, *11*(390), 1–11. https://doi.org/10.3389/fncel.2017.00390

Kano, O., Tanaka, K., Kanno, T., Iwasaki, Y., & Ikeda, J. E. (2018). Neuronal apoptosis inhibitory protein is implicated in amyotrophic lateral sclerosis symptoms. *Scientific Reports*, *8*(1), 6. https://doi.org/10.1038/s41598-017-18627-w

Kawabori, M., & Yenari, M. A. (2015). The role of the microglia in acute CNS injury. *Metabolic Brain Disease*, *30*(2), 381–392. https://doi.org/10.1007/s11011-014-9531-6

Kim, C. M., Alvarado, R. L., Stephens, K., Wey, H. Y., Wang, D. J. J., Leritz, E. C., & Salat, D. H. (2020). Associations between cerebral blood flow and structural and functional brain imaging measures in individuals with neuropsychologically defined mild cognitive impairment. *Neurobiology of Aging*, *86*, 64–74. https://doi.org/10.1016/j.neurobiolaging.2019.10.023

Kim, J. Y., Kim, J. H., Kim, Y. D., & Seo, J. H. (2020). High vulnerability of oligodendrocytes to oxidative stress induced by ultrafine urban particles. *Antioxidants (Basel)*, *10*(1), 4. https://doi.org/10.3390/antiox10010004

Koppal, T., Drake, J., Yatin, S., Jordan, B., Varadarajan, S., Bettenhausen, L., & Butterfield, D. A. (1999). Peroxynitrite-induced alterations in synaptosomal membrane proteins: Insight into oxidative stress in Alzheimer's disease. *Journal of Neurochemistry*, *72*(1), 310–317.

Kulick, E. R., Elkind, M. S. V., Boehme, A. K., Joyce, N. R., Schupf, N., Kaufman, J. D., Mayeux, R., Manly, J. J., & Wellenius, G. A. (2020). Long-term exposure to ambient air pollution, APOE-ε4 status, and cognitive decline in a cohort of older adults in northern Manhattan. *Environment International*, *136*, 105440. https://doi.org/10.1016/j.envint.2019.105440

Kyrylkova, K., Kyryachenko, S., Leid, M., & Kioussi, C. (2012). Detection of apoptosis by TUNEL assay. *Methods in Molecular Biology*, *887*, 41–47. https://doi.org/10.1007/978-1-61779-860-3_5

Lassmann, H., & van Horssen, J. (2016). Oxidative stress and its impact on neurons and glia in multiple sclerosis lesions. *Biochimica et Biophysica Acta*, *1862*(3), 506–510. https://doi.org/10.1016/j.bbadis.2015.09.018

Li, J., Baud, O., Vartanian, T., Volpe, J. J., & Rosenberg, P. A. (2005). Peroxynitrite generated by inducible nitric oxide synthase and NADPH oxidase mediates microglial toxicity to oligodendrocytes. *Proceedings of the National Academy of Sciences of the United States of America*, *102*(28), 9936–9941.

Li, Y., Liu, S. L., & Qi, S. H. (2018). ALDH2 protects against ischemic stroke in rats by facilitating 4-HNE clearance and AQP4 down-regulation. *Neurochemical Research*, *43*(7), 1339–1347. https://doi.org/10.1007/s11064-018-2549-0

Liguori, I., Russo, G., Curcio, F., Bulli, G., Aran, L., Della-Morte, D., Gargiulo, G., Testa, G., Cacciatore, F., Bonaduce, D., & Abete, P. (2018). Oxidative stress, aging, and diseases. *Clinical Interventions in Aging*, *13*, 757–772. https://doi.org/10.2147/cia.S158513

Lim, J. L., Van der Pol, S. M. A., Baron, W., McCord, J. M., De Vries, H. E., & Van Horssen, J. (2016). Protandim protects oligodendrocytes against an oxidative insult. *Antioxidants*, *5*(3), 30.

Liu, Q., Babadjouni, R., Radwanski, R., Cheng, H., Patel, A., Hodis, D. M., He, S., Baumbacher, P., Russin, J. J., Morgan, T. E., Sioutas, C., Finch, C. E., & Mack, W. J. (2016). Stroke damage is exacerbated

by nano-size particulate matter in a mouse model. *PLoS One*, *11*(4), e0153376. https://doi.org/10.1371/journal.pone.0153376

Liu, Q., He, S., Groysman, L., Shaked, D., Russin, J., Scotton, T. C., Cen, S., & Mack, W. J. (2013). White matter injury due to experimental chronic cerebral hypoperfusion is associated with C5 deposition. *PLoS One*, *8*(12), e84802. https://doi.org/10.1371/journal.pone.0084802

Liu, Q., Radwanski, R., Babadjouni, R., Patel, A., Hodis, D. M., Baumbacher, P., Zhao, Z., Zlokovic, B., & Mack, W. J. (2019). Experimental chronic cerebral hypoperfusion results in decreased pericyte coverage and increased blood-brain barrier permeability in the corpus callosum. *Journal of Cerebral Blood Flow and Metabolism*, *39*(2), 240–250. https://doi.org/10.1177/0271678x17743670

Liu, Q., Shkirkova, K., Lamorie-Foote, K., Connor, M., Patel, A., Babadjouni, R., Huuskonen, M., Montagne, A., Baertsch, H., Zhang, H., Chen, J. C., Mack, W. J., Walcott, B. P., Zlokovic, B. V., Sioutas, C., Morgan, T. E., Finch, C. E., & Mack, W. J. (2021). Air pollution particulate matter exposure and chronic cerebral hypoperfusion and measures of white matter injury in a murine model. *Environmental Health Perspectives*, *129*(8), 87006. https://doi.org/10.1289/ehp8792

Lloret, A., Esteve, D., Lloret, M. A., Monllor, P., López, B., León, J. L., & Cervera-Ferri, A. (2021). Is oxidative stress the link between cerebral small vessel disease, sleep disruption, and oligodendrocyte dysfunction in the onset of Alzheimer's disease? *Frontiers in Physiology*, *12*(1330), 1–10. https://doi.org/10.3389/fphys.2021.708061

McCracken, E., Valeriani, V., Simpson, C., Jover, T., McCulloch, J., & Dewar, D. (2000). The lipid peroxidation by-product 4-hydroxynonenal is toxic to axons and oligodendrocytes. *Journal of Cerebral Blood Flow and Metabolism*, *20*(11), 1529–1536. https://doi.org/10.1097/00004647-200011000-00002

Mirzayans, R., & Murray, D. (2020). Do TUNEL and other apoptosis assays detect cell death in preclinical studies? *International Journal of Molecular Sciences*, *21*(23), 9090. https://doi.org/10.3390/ijms21239090

Misra, C., Kim, S., Shen, S., & Sioutas, C. (2002). A high flow rate, very low pressure drop impactor for inertial separation of ultrafine from accumulation mode particles. *Journal of Aerosol Science*, *33*(5), 735–752. https://doi.org/10.1016/S0021-8502(01)00210-5

Miyamoto, N., Maki, T., Pham, L. D., Hayakawa, K., Seo, J. H., Mandeville, E. T., Mandeville, J. B., Kim, K. W., Lo, E. H., & Arai, K. (2013). Oxidative stress interferes with white matter renewal after prolonged cerebral hypoperfusion in mice. *Stroke*, *44*(12), 3516–3521. https://doi.org/10.1161/strokeaha.113.002813

Morgan, T. E., Davis, D. A., Iwata, N., Tanner, J. A., Snyder, D., Ning, Z., Kam, W., Hsu, Y. T., Winkler, J. W., Chen, J. C., Petasis, N. A., Baudry, M., Sioutas, C., & Finch, C. E. (2011). Glutamatergic neurons in rodent models respond to nanoscale particulate urban air pollutants in vivo and in vitro. *Environmental Health Perspectives*, *119*(7), 1003–1009. https://doi.org/10.1289/ehp.1002973

Nishioku, T., Matsumoto, J., Dohgu, S., Sumi, N., Miyao, K., Takata, F., Shuto, H., Yamauchi, A., & Kataoka, Y. (2010). Tumor necrosis factor-α mediates the blood–brain barrier dysfunction induced by activated microglia in mouse brain microvascular endothelial cells. *Journal of Pharmacological Sciences*, *112*(2), 251–254. https://doi.org/10.1254/jphs.09292SC

Patel, A., Moalem, A., Cheng, H., Babadjouni, R. M., Patel, K., Hodis, D. M., Chandegara, D., Cen, S., He, S., Liu, Q., & Mack, W. J. (2017). Chronic cerebral hypoperfusion induced by bilateral carotid artery stenosis causes selective recognition impairment in adult mice. *Neurological Research*, *39*(10), 910–917. https://doi.org/10.1080/01616412.2017.1355423

Peters, R., Ee, N., Peters, J., Booth, A., Mudway, I., & Anstey, K. J. (2019). Air pollution and dementia: A systematic review. *Journal of Alzheimer's Disease*, *70*(s1), S145–S163. https://doi.org/10.3233/jad-180631

Petkus, A. J., Younan, D., Widaman, K., Gatz, M., Manson, J. E., Wang, X., Serre, M., Vizuete, W., Chui, H., Espeland, M. A., Resnick, S., & Chen, J. C. (2020). Exposure to fine particulate matter and temporal dynamics of episodic memory and depressive symptoms in older women. *Environment International*, *135*, 105196. https://doi.org/10.1016/j.envint.2019.105196

Pirhadi, M., Mousavi, A., Sowlat, M. H., Janssen, N. A. H., Cassee, F. R., & Sioutas, C. (2020). Relative contributions of a major international airport activities and other urban sources to the particle number concentrations (PNCs) at a nearby monitoring site. *Environmental Pollution*, *260*, 114027. https://doi.org/10.1016/j.envpol.2020.114027

Poh, L., Fann, D. Y., Wong, P., Lim, H. M., Foo, S. L., Kang, S. W., Rajeev, V., Selvaraji, S., Iyer, V. R., Parathy, N., Khan, M. B., Hess, D. C., Jo, D. G., Drummond, G. R., Sobey, C. G., Lai, M. K. P., Chen, C. L., Lim, L. H. K., & Arumugam, T. V. (2020). AIM2 inflammasome mediates hallmark neuropathological alterations and cognitive impairment in a mouse model of vascular dementia. *Molecular Psychiatry*, *26*, 4544–4560. https://doi.org/10.1038/s41380-020-00971-5

Poli, G., & Schaur, R. J. (2000). 4-Hydroxynonenal in the pathomechanisms of oxidative stress. *IUBMB Life*, *50*(4–5), 315–321. https://doi.org/10.1080/713803726

Radi, E., Formichi, P., Battisti, C., & Federico, A. (2014). Apoptosis and oxidative stress in neurodegenerative diseases. *Journal of Alzheimer's Disease*, *42*(Suppl 3), S125–S152. https://doi.org/10.3233/jad-132738

Saffari, A., Daher, N., Shafer, M. M., Schauer, J. J., & Sioutas, C. (2013). Seasonal and spatial variation of trace elements and metals in quasi-ultrafine ($PM_{0.25}$) particles in the Los Angeles metropolitan area and characterization of their sources. *Environmental Pollution*, *181*, 14–23. https://doi.org/10.1016/j.envpol.2013.06.001

Saha, R. N., & Pahan, K. (2006). Regulation of inducible nitric oxide synthase gene in glial cells. *Antioxidants & Redox Signaling*, *8*(5–6), 929–947. https://doi.org/10.1089/ars.2006.8.929

Sardar, S. B., Fine, P. M., & Sioutas, C. (2005). Seasonal and spatial variability of the size-resolved chemical composition of particulate matter (PM10) in the Los Angeles Basin. *Journal of Geophysical Research: Atmospheres*, *110*(D7), 1–14. https://doi.org/10.1029/2004JD004627

Shibata, M., Ohtani, R., Ihara, M., & Tomimoto, H. (2004). White matter lesions and glial activation in a novel mouse model of chronic cerebral hypoperfusion. *Stroke*, *35*(11), 2598–2603. https://doi.org/10.1161/01.Str.0000143725.19053.60

Shirmohammadi, F., Hasheminassab, S., Saffari, A., Schauer, J. J., Delfino, R. J., & Sioutas, C. (2016). Fine and ultrafine particulate organic carbon in the Los Angeles basin: Trends in sources and composition. *Science of the Total Environment*, *541*, 1083–1096. https://doi.org/10.1016/j.scitotenv.2015.09.133

Sonar, S. A., & Lal, G. (2019). The iNOS activity during an immune response controls the CNS pathology in experimental autoimmune encephalomyelitis. *Frontiers in Immunology*, *10*, 710. https://doi.org/10.3389/fimmu.2019.00710

Sowlat, M. H., Hasheminassab, S., & Sioutas, C. (2016). Source apportionment of ambient particle number concentrations in central Los Angeles using positive matrix factorization (PMF). *Atmospheric Chemistry and Physics*, *16*(8), 4849–4866. https://doi.org/10.5194/acp-16-4849-2016

Sozmen, E. G., Rosenzweig, S., Llorente, I. L., DiTullio, D. J., Machnicki, M., Vinters, H. V., Havton, L. A., Giger, R. J., Hinman, J. D., & Carmichael, S. T. (2016). Nogo receptor blockade overcomes remyelination failure after white matter stroke and stimulates functional recovery in aged mice. *Proceedings of the National Academy of Sciences of the United States of America*, *113*(52), E8453–E8462. https://doi.org/10.1073/pnas.1615322113

Spaas, J., van Veggel, L., Schepers, M., Tiane, A., van Horssen, J., Wilson, D. M., Moya, P. R., Piccart, E., Hellings, N., Eijnde, B. O., Derave, W., Schreiber, R., & Vanmierlo, T. (2021). Oxidative stress and impaired oligodendrocyte precursor cell differentiation in neurological disorders. *Cellular and Molecular Life Sciences*, *78*(10), 4615–4637. https://doi.org/10.1007/s00018-021-03802-0

Stewart, C. R., Stuart, L. M., Wilkinson, K., van Gils, J. M., Deng, J., Halle, A., Rayner, K. J., Boyer, L., Zhong, R., Frazier, W. A., Lacy-Hulbert, A., El Khoury, J., Golenbock, D. T., & Moore, K. J. (2010). CD36 ligands promote sterile inflammation through assembly of a Toll-like receptor 4 and 6 heterodimer. *Nature Immunology*, *11*(2), 155–161. https://doi.org/10.1038/ni.1836

Sweeney, M. D., Montagne, A., Sagare, A. P., Nation, D. A., Schneider, L. S., Chui, H. C., Harrington, M. G., Pa, J., Law, M., Wang, D. J. J., Jacobs, R. E., Doubal, F. N., Ramirez, J., Black, S. E., Nedergaard, M., Benveniste, H., Dichgans, M., Iadecola, C., Love, S., ... Zlokovic, B. V. (2019). Vascular dysfunction—The disregarded partner of Alzheimer's disease. *Alzheimer's & Dementia*, *15*(1), 158–167. https://doi.org/10.1016/j.jalz.2018.07.222

Taghvaee, S., Mousavi, A., Sowlat, M. H., & Sioutas, C. (2019). Development of a novel aerosol generation system for conducting inhalation exposures to ambient particulate matter (PM). *Science of the Total Environment*, *665*, 1035–1045. https://doi.org/10.1016/j.scitotenv.2019.02.214

Thorburne, S. K., & Juurlink, B. H. (1996). Low glutathione and high iron govern the susceptibility of oligodendroglial precursors to oxidative stress. *Journal of Neurochemistry*, *67*(3), 1014–1022. https://doi.org/10.1046/j.1471-4159.1996.67031014.x

Tsai, T. L., Lin, Y. T., Hwang, B. F., Nakayama, S. F., Tsai, C. H., Sun, X. L., Ma, C., & Jung, C. R. (2019). Fine particulate matter is a potential determinant of Alzheimer's disease: A systemic review and meta-analysis. *Environmental Research*, *177*, 108638. https://doi.org/10.1016/j.envres.2019.108638

Turpin, B. J., & Lim, H.-J. (2001). Species contributions to PM2.5 mass concentrations: Revisiting common assumptions for estimating organic mass. *Aerosol Science and Technology*, *35*(1), 602–610. https://doi.org/10.1080/02786820119445

van Dalen, J. W., Mutsaerts, H., Nederveen, A. J., Vrenken, H., Steenwijk, M. D., Caan, M. W. A., Majoie, C. B. L. M., van Gool, W. A., & Richard, E. (2016). White matter hyperintensity volume and cerebral perfusion in older individuals with hypertension using arterial spin-labeling. *AJNR. American Journal of Neuroradiology*, *37*(10), 1824–1830. https://doi.org/10.3174/ajnr.A48282016

Woodward, N. C., Levine, M. C., Haghani, A., Shirmohammadi, F., Saffari, A., Sioutas, C., Morgan, T. E., & Finch, C. E. (2017). Toll-like receptor 4 in glial inflammatory responses to air pollution in vitro and in vivo. *Journal of Neuroinflammation*, *14*(1), 84. https://doi.org/10.1186/s12974-017-0858-x

Woodward, N. C., Pakbin, P., Saffari, A., Shirmohammadi, F., Haghani, A., Sioutas, C., Cacciottolo, M., Morgan, T. E., & Finch, C. E. (2017). Traffic-related air pollution impact on mouse brain accelerates myelin and neuritic aging changes with specificity for CA1 neurons. *Neurobiology of Aging*, *53*, 48–58. https://doi.org/10.1016/j.neurobiolaging.2017.01.007

Younan, D., Petkus, A. J., Widaman, K. F., Wang, X., Casanova, R., Espeland, M. A., Gatz, M., Henderson, V. W., Manson, J. E., Rapp, S. R., Sachs, B. C., Serre, M. L., Gaussoin, S. A., Barnard, R., Saldana, S., Vizuete, W., Beavers, D. P., Salinas, J. A., Chui, H. C., ... Chen, J. C. (2020). Particulate matter and episodic memory decline mediated by early neuroanatomic biomarkers of Alzheimer's disease. *Brain*, *143*(1), 289–302. https://doi.org/10.1093/brain/awz348

Zhang, H., D'Agostino, C., Forman, H. J., Cacciottolo, M., Thorwald, M., Mack, W. J., Liu, Q., Shkirkova, K., Lamorie-Foote, K., Sioutas, C., Pirhadi, M., Mack, W. J., Morgan, T. E., & Finch, C. E. (2021). Urban air pollution nanoparticles from Los Angeles: Recently decreased neurotoxicity. *Journal of Alzheimer's Disease*, *82*(1), 307–316. https://doi.org/10.3233/JAD-201577

Zhang, S., Eitan, E., & Mattson, M. P. (2017). Early involvement of lysosome dysfunction in the degeneration of cerebral cortical neurons caused by the lipid peroxidation product 4-hydroxynonenal. *Journal of Neurochemistry*, *140*(6), 941–954. https://doi.org/10.1111/jnc.13957

Zhang, T., Zheng, X., Wang, X., Zhao, H., Wang, T., Zhang, H., Li, W., Shen, H., & Yu, L. (2018). Maternal exposure to PM(2.5) during pregnancy induces impaired development of cerebral cortex in mice offspring. *International Journal of Molecular Sciences*, *19*(1), 257. https://doi.org/10.3390/ijms19010257

Zhang, X., Kimura, Y., Fang, C., Zhou, L., Sfyroera, G., Lambris, J. D., Wetsel, R. A., Miwa, T., & Song, W. C. (2007). Regulation of Toll-like receptor-mediated inflammatory response by complement in vivo. *Blood*, *110*(1), 228–236. https://doi.org/10.1182/blood-2006-12-063636

Zheng, X., Wang, X., Wang, T., Zhang, H., Wu, H., Zhang, C., Yu, L., & Guan, Y. (2019). Gestational exposure to particulate matter 2.5 (PM2.5) leads to spatial memory dysfunction and neurodevelopmental impairment in hippocampus of mice offspring. *Frontiers in Neuroscience*, *12*(1000), 1–18. https://doi.org/10.3389/fnins.2018.01000

SUPPORTING INFORMATION

Additional supporting information can be found online in the Supporting Information section at the end of this article.

FIGURE S1 TNFα brain hemisphere western blot
TABLE S1 Antibody table